Ember Aviation

Presents the

LAT-1

In response to the 2015 – 2016 AIAA Foundation Undergraduate Team

Aircraft Design Competition

Presented by California Polytechnic State University, Pomona

Aerospace Engineering Department

Aircraft Design 2015 – 2016

CAL POLY POMONA

Ember Aviation Team

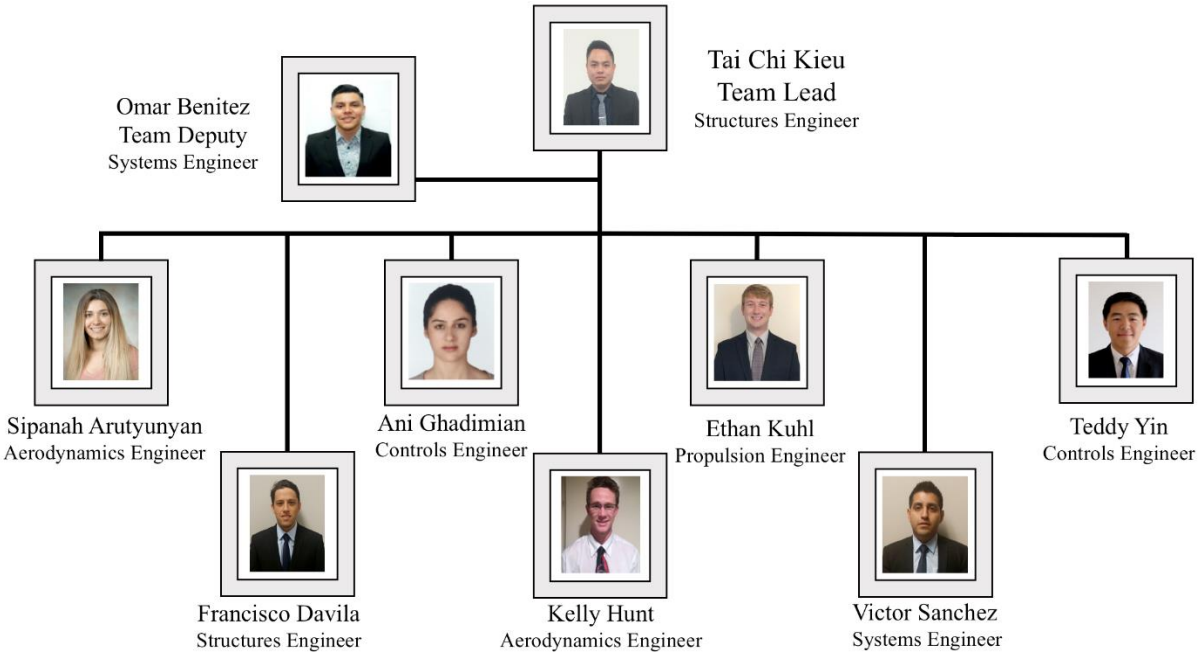

Team AIAA Member Numbers

Arutyunyan, Sipanah	Aerodynamics	688353	sipanah@gmail.com
Benitez, Omar	Team Deputy, Systems	688415	benitez@cpp.edu
Davila, Francisco	Structures	688424	franciscor_d@yahoo.com

Ghadimian, Ani	Controls	481732	ani.masihi@gmail.com

Hunt, Kelly	Aerodynamics	688649	kchunt@cpp.edu

Kieu, Tai Chi	Team Lead, Structures	605712	tckieu@cpp.edu

Kuhl, Ethan	Propulsion	688654	ethankuhl941@gmail.com

Sanchez, Victor	Systems Engineering	688422	v.sanchez91@yahoo.com

Yin, Teddy	Controls	665617	teddyyin@gmail.com

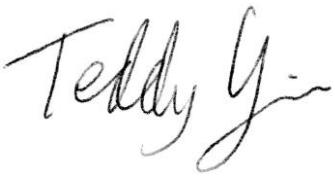

Dr. Don Edberg	Design Advisor	022972-00	dedberg@cpp.edu

Executive Summary

In response to the 2015-2016 American Institute of Aeronautics and Astronautics (AIAA) Graduate Team Aircraft Design Competition Request for Proposal, Ember Aviation would like to present the LAT-1. The Ember Aviation team which consists of Aerospace Engineering undergraduate students currently attending California Polytechnic State University, Pomona received the RFP on September 2015. The RFP states that Researchers at NASA have predicted an increase in wildfires during the next 50-100 years due to the increase in global temperatures. In result, the need for a purpose built aircraft to fight wildfires is more apparent. The RFP requested a design of a Large Air Tanker with an Entry into Service date of 2022 with a lifetime of no less than 20 years. This purposely built Large Air Tanker will replace current retrofitted aircraft that are in service today. According to the RFP, one of the mission that this design should perform is that the aircraft shall be able to carry a payload of 5,000 gallons of water or retardant that is equivalent to a max weight of 45,000 lbs. to perform 3 drops per sortie (assumed 4 sorties per the RFP) on a 200 nm radius from base. Another mission the design shall be able to perform is to perform a Ferry Range of 2,500 nm. During the drop mission, the LAT-1 will cruise when flying to the fire site, and it will drop the retardant below 300 ft. above ground level at a speed less than 150 knots to have retardant shear minimized and accuracy increased. The bases at which the aircraft will be taking off and landing have a Balanced Field Length of 5,000 ft. with an assumption of +35°F standard atmosphere at an altitude of 5,000 ft. above mean sea-level. The aircraft shall minimize total ownership cost and shall be equipped with sensors, cameras, communication equipment, etc., all to provide a forward observer function for other firefighting aircraft in the area. The LAT-1 aircraft design submitted by Ember Aviation, features a retardant tank fuselage shape with two engines mounted on top of the wings.

W_{TO} = 89,076 lb	W_{TO}/S = 48 psf
$t/c)_{ave}$ = .15	T_{SL}/W_{TO} = .44
b = 122.2 ft	Length = 68 ft
C = 16.2 ft	Sweep = 3 deg
S_{ref} = 1868	CG = 19 ft

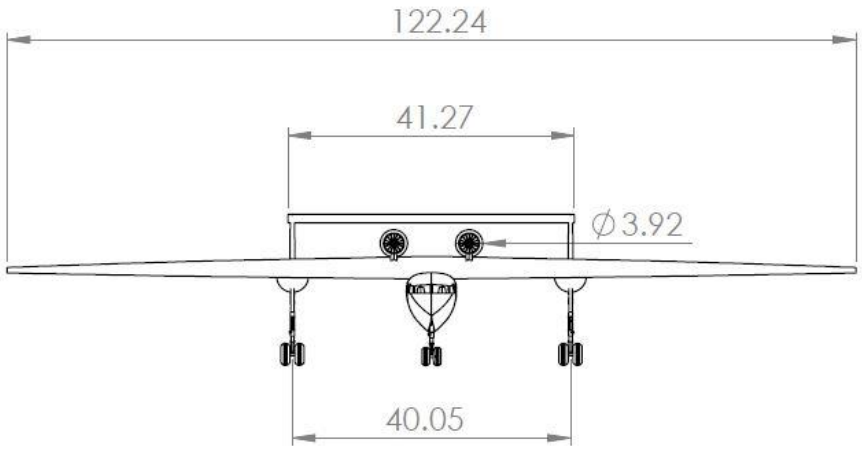

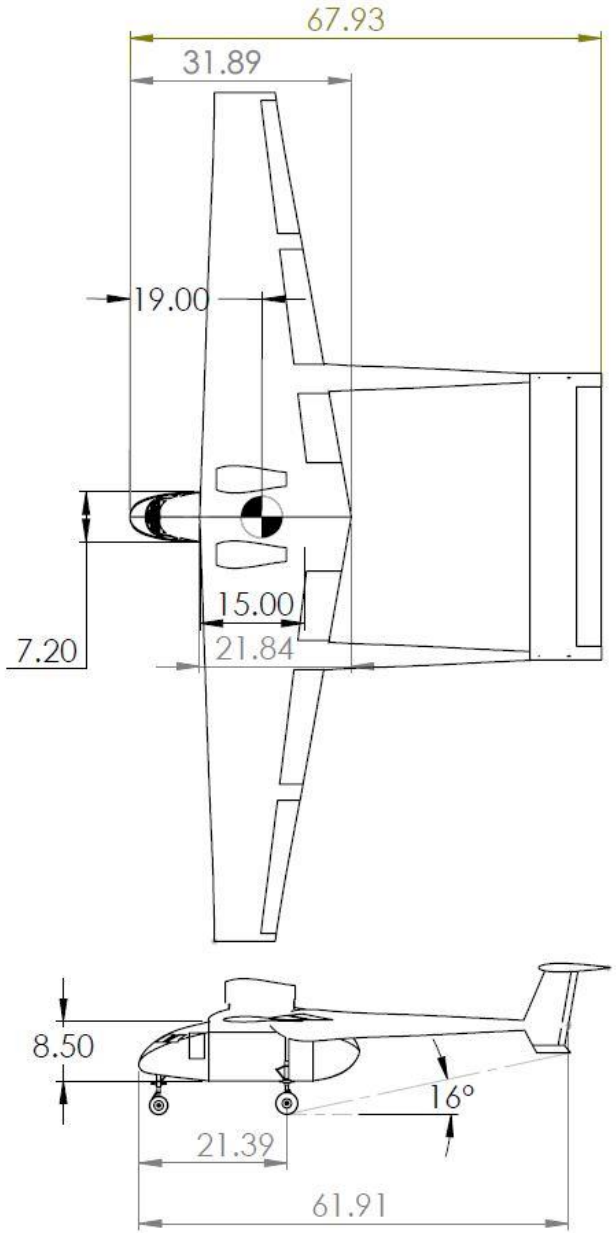

Table of Contents

List of Figures

List of Tables

List of Acronyms

AIAA:	American Institute of Aeronautics and Astronautics
CG:	center of gravity
BFL:	balanced field length
D.O.C:	direct operating cost
ECS:	environmental control system
EIS:	entry into service
FEA:	finite element analysis
MAC:	mean aerodynamic chord
MTOW:	max takeoff weight
ROC:	rate of climb
SFC:	specific fuel consumption
SSL:	standard sea level
V_{S1}:	1 g stall speed
V_{Sneg}:	negative stall speed
V_A:	design maneuvering speed
V_B:	design max gust intensity speed
V_C:	design cruising speed
V_D:	design diving speed

1. Requirement Overview

The LAT-1 will enter into service in the year 2022 with a lifetime of no less than 20 years. Perhaps the most important requirement by the RFP from AIAA is the ability of carrying a payload of 45,000 lbs. for an operational radius of 200 nm. The aircraft shall be able to have a crew of 2 pilots. The ground support equipment shall have the capability of reloading retardant in less than 10 minutes. It shall be equipped with sensors, communication systems, etc., all to provide communication with any firefighting aircraft nearby. When performing the drops, the LAT-1 will drop the retardant below 300 ft. above ground level at a speed less than 150 knots but no less than 90 knots because of a stall speed requirement. When the aircraft drops and is now empty, it shall dash back to base at a speed greater than 300 knots. It is asked to look into both a turboprop and turbofan engines with the preference of choosing an off-the-shelf engine. There is a ferry range requirement of 2,500 nm to provide the aircraft to any state within the United States that is experiencing a wildfire. The balanced field length is 5,000 ft. with an assumption of +35°F standard atmosphere at an altitude of 5,000 ft. above mean sea-level. It shall minimize total ownership cost with justification of the acquisition of the greater capability instead of having a retrofitted aircraft. Finally, the aircraft shall be FAA approved with certification of transfer aircraft (Part 25) with an emphasis on fatigue.

2. Configuration Overview

2.1 Configuration Concept

The key driving concept for our aircraft, was a mindset we called, *Size Zero*. The idea behind this was to eliminate any and all wasted space within the aircraft. The goal for our team was to utilize every inch within the aircraft, hence the s*ize zero* name for this design concept, in which there was zero wasted space within the airframe. One obvious downfall with all of the current retrofit aircraft currently in operation as firefighting aircraft, is that the payload tanks and drop mechanisms are often attached underneath the fuselage of the aircraft, or occupy very little space within the aircraft. This leads to excess wasted space, wasted space that the aircraft operators are paying for on every flight. By keeping wasted space within the aircraft to minimum, we can prevent excess structural weight and wetted area on the aircraft. Our team stayed focused on making sure that every component installed on the aircraft, earned its way on to the aircraft structure.

This *size zero* mindset heavily influenced the manner in which the payload tank and cockpit were integrated into the aircraft. The aft section of the fuselage is nothing more than the payload tank itself, hung from the primary wing spars. The cockpit, similarly, is attached onto the front of the payload tank with no wasted surface area on the aircraft.

2.2 Twin Boom Tail

Given our effort to eliminate wasted space, more specifically the aft fuselage that must be in place to support the vertical and horizontal tails, a different kind of tail must be designed. In the case of our aircraft, a twin-boom tail was deemed to be an ideal solution to this problem. A twin

boom tail not only allows for the elevator to place up high in free-stream clean air, thus increasing the efficiency of the horizontal stabilizer, but also allows for a smaller overall vertical tail area, given that there are two vertical surfaces, as opposed to a single tail surface. Given the heavy payload, the larger the elevator, generally the better the aircraft takeoff performance is. By utilizing this twin-boom design, a significantly larger horizontal stabilizer can be design, without creating a difficult structures problem for supporting a tail that large and heavy on a conventional "cigar tube" aircraft. Our aircraft also is unlikely to be ever be reconfigured for any duty, other than that of a fire fighting, thus eliminating the necessity for reconfigurable aft fuselage space.

3. Material Selection

One of the main requirements mentioned in the RFP is special attention to FFA certification for transport aircraft (Part 25) fatigue. Failure by fatigue is perhaps the biggest concern for structural failure for aircraft components, and it occurs when exposed to frequent applied load. These critical areas can be found on different structural paths and they should be carefully monitored to prevent cracks from stress concentration. Structural Health Monitoring (SHM) is considered one of the most reliable technologies that can be used for early detection of the cracks.

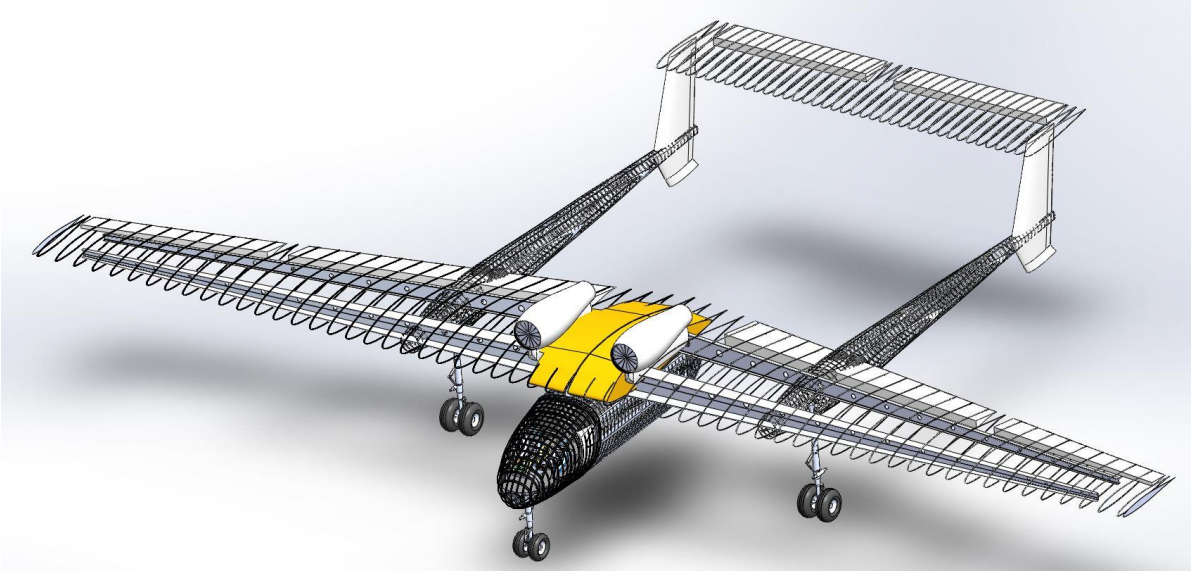

Figure 3-1: A preliminary of materials for the LAT-1 structure was determined

Therefore, to begin the material selection process, different aircraft materials were examined. DC-10 which is an operating air-tanker, capable of carrying 12,000 gallon of retardant, uses aluminum 2024-T3. This material is widely used in aerospace application due to its excellent fatigue strength, fracture toughness and notch sensitivity. Some of the properties of Aluminum 2024-T3 include fatigue strength of 140 MPa, fracture toughness of 25 MPa-$m^{1/2}$, tensile strength of 483 MPa, and high tensile yield strength of 345 MPa. This material will be used in the areas

with the highest tension such as the lower wing skin, and pressure critical fuselage skins where fatigue is an important driver. There is a study done on aluminum alloy 2024-T3 for airbus A320 slat-track. The result shows that using SHM technology and electrical conductivity due to the crack growth, the fatigue failure can be easily monitored.

4. Mission Analysis

The RFA requested that the Large Air Taker being designed shall be able to carry 5,000 gallons of water or retardant (retardant weighing 9 pounds per gallon). This makes the payload weight come out to be a total of 45,000 lbs. When attacking a wildfire, the aircraft will be taking off from an altitude of 5,000 ft. and shall be able to perform 4 sorties on a 200 nm radius (from base) per sortie with the capability of performing 3 retardant or water drops during each sortie while it is establishing the best fire line to prevent the fire from expanding. In addition to this mission, the RFA also required that the aircraft shall be able to perform a ferry range of 2,500 nm in order to lend the aircraft to any state in the United States if that states was experiencing a wildfire. The mission profiles of this Large Air Tanker can be seen in Figure 4-1, Figure 4-2, and Figure 4-3. Also, the fuel burned during this mission is listed in Table 5-1 below.

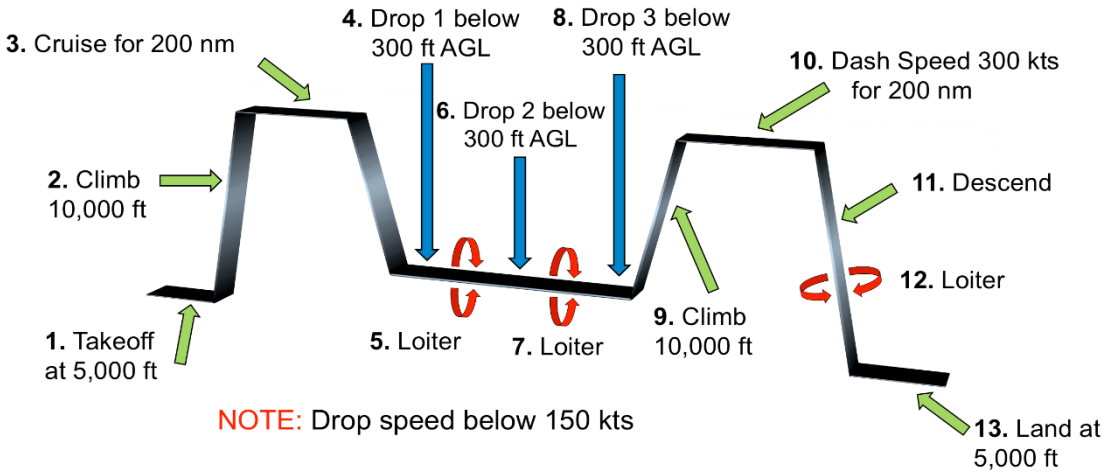

Figure 4-1: Mission Profile 1 of the LAT-1 will perform 1 sortie and 3 retardant drops

In Mission Profile 1, the aircraft will fly out to the fire site on a 200 nm radius from the airport it is taking off from. It is estimated that the aircraft will climb 10,000 ft., cruise at a speed of 250 kts for 200 nm to the fire site, descend and perform 3 drops of retardant and all 3 drops

must be dropped below 300 ft. above ground level and a speed lower than 150 knots for accuracy. After the drops have been performed, the aircraft will climb 10,000 ft. and dash with a speed greater than 300 kts back to base for a reload of retardant that will be performed in 4 minutes while the engines are idling. Once the aircraft is reloaded with retardant, it will takeoff once again to the fire site. It is assumed from the RFP that 4 sorties can establish a fire line to prevent the fire from expanding.

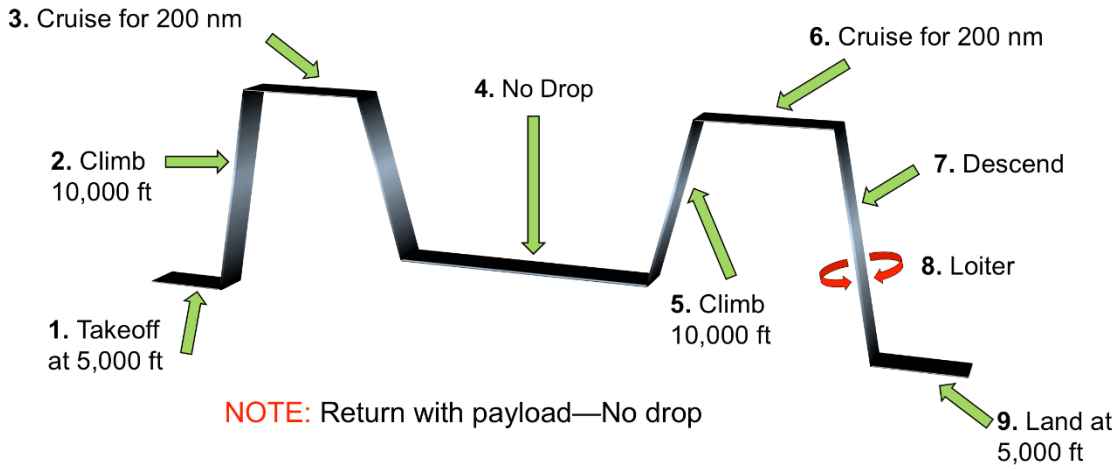

Figure 4-2: Mission Profile 2 of the LAT-1 will not drop payload and return to base

In Mission Profile 2, the aircraft will takeoff from base just like in Mission Profile 1 and cruise to the fire site on a 200 nm radius from which the aircraft takes off from. The only difference with this mission compared to the first mission is that there will be no retardant drop. The reason why there will be no retardant drop is that perhaps there was a malfunction with the hydraulic doors, or there was no need for dropping retardant anymore. If this scenario occurs, the aircraft will return to base with its full payload of 45,000 lbs. It is this scenario that resulted in our aircraft being the heaviest.

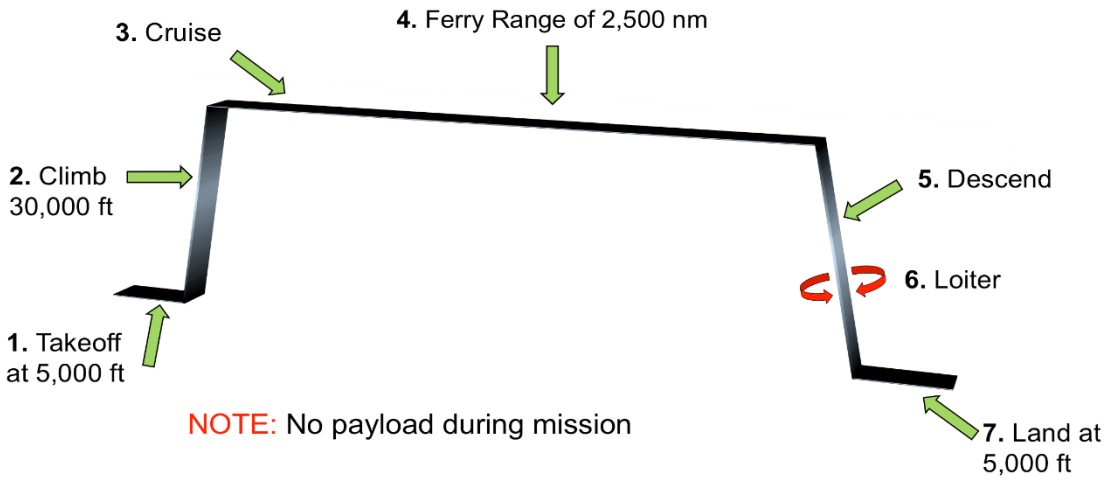

Figure 4-3: Mission Profile 3 of the LAT-1 will perform a 2,500 nm ferry range empty

In Mission Profile 3, the aircraft will be performing its ferry range distance of 2,500 nm. The aircraft shall be able to be dispatched quickly anywhere to the continental United States if there is need of a fire fighting aircraft. During this mission, the aircraft will be flying empty (no retardant) because there is no need to fly the aircraft loaded; it will only result in unnecessary fuel burning, thus causing our aircraft to be even heavier. That being said, the aircraft will climb to 30,000 ft. for the turbofan engines to fly at their best efficiency. The aircraft will not be pressurized; however, we will have oxygen masks provided to the pilots in order for them to breathe oxygen with ease. Once the aircraft reaches its altitude, the ferry range mission of 2,500 nm will be performed as the aircraft cruises at 250 nm. Once the aircraft arrives to its destination, it will loiter before landing if necessary.

5. Design Approach

In designing the LAT-1, much attention was paid to minimizing the cost. The ultimate objective was for the design to meet all of the requirements described in section 1.0 in the most cost effective way. It was well noted that greatly exceeding the requirements would likely drive up the cost. Therefore, careful and detailed analysis was done to ensure that the requirements are met without being greatly exceeded. In order to ensure that the requirements are being met, a constraint diagram was constructed to indicate the optimal thrust-to-weight and wing loading. In order to ensure that the requirements are not being greatly exceeded, a carpet plot was constructed illustrating the results of the design process from multiple iterations, which was used to determine the optimal wing aspect ratio and engine for the aircraft.

5.1 Initial Sizing

The initial size of the aircraft was determined based on the performance requirements specified by the RFP. The dash speed, balanced field length, and stall speed requirements were all addressed in determining the optimal thrust-to-weight and wing loading of the aircraft. The constraint diagram, shown in Figure 5.1-1, was constructed with curves representing the boundaries of the possible design space for which the aircraft will meet these requirements.

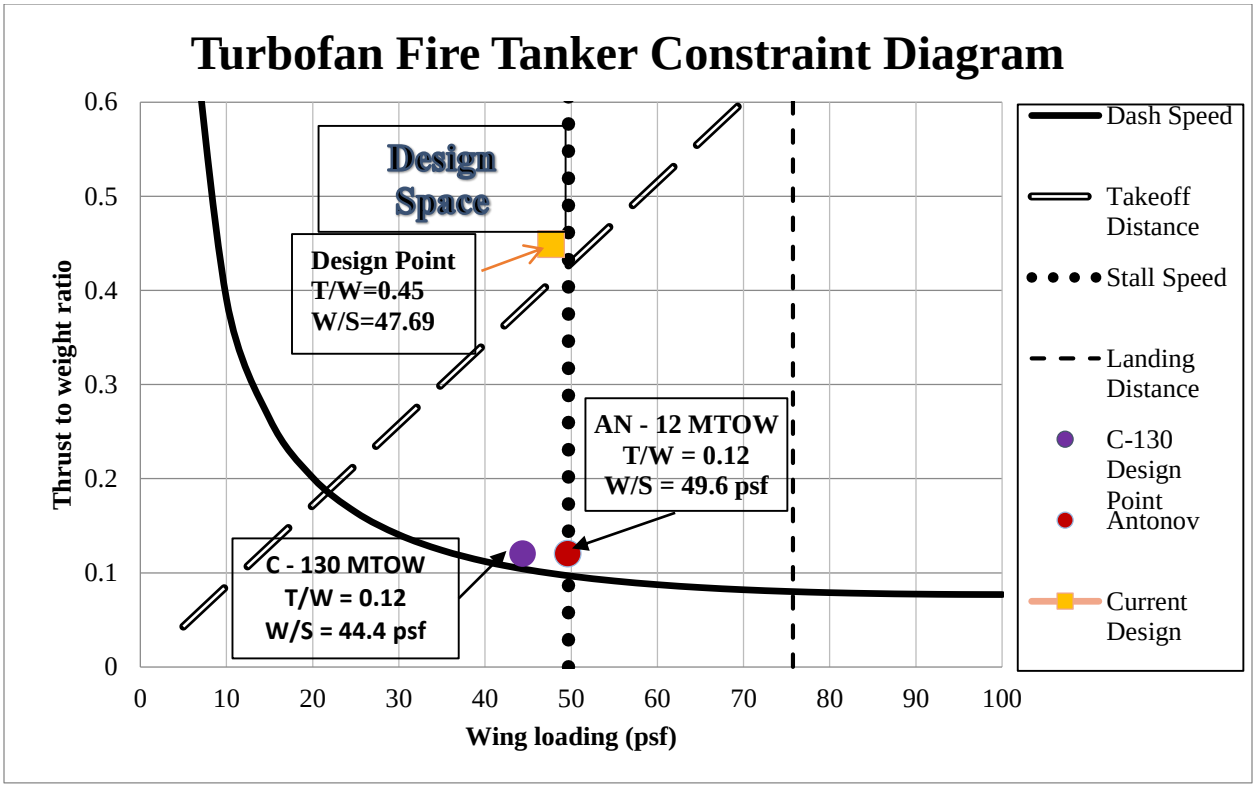

Figure 5.1-1: Constraint Diagram

The design point was targeted to lie in the rightmost and bottommost location of the design space. The rightmost location is desired because a higher wing loading signifies a smaller wing area, which minimizes cost. Also, it is stated in Schaufele [3]'s Fig. 4-1 that a typical wing loading for a short to medium range jet transport is in the range of 80-120 psf. This range clearly lies outside of the design space, which is due to our stall speed constraint. However, the rightmost location within the design space results in a wing loading that is closest to that of similar aircraft. The bottommost location was desired because a lower thrust-to-weight ratio signifies an engine with a lower thrust which generally has a lower cost. The design point, as indicated by a yellow square, specifies a thrust-to-weight ratio of 0.45 and a wing loading of 47.69 psf. For comparison, the Lockheed C-130 and Antonov An-12 are also shown on the graph.

5.2 Iteration and Refinement

In an effort to design the most ideal aircraft for the mission, the team carried out many iterations and continuously refined the aircraft. The conceptual design phase was performed 12 times by varying the aspect ratio of the wing and engine selection. The aspect ratio was varied from 8 to 12 and the engine was varied between four variants of the GE CF34: the CF34-8C5, -8E, -10A, and -10E, which produce different static thrusts with minimal change in weight. The GE engine was down-selected from a number of possible engines that yield a thrust-to-weight ratio of about 0.45. (Note: a more detailed explanation of the engine trade study can be found in Section 9.1). In the process of these iterations, data was collected and analyzed to see which combination of aspect ratio and engine results in the best airplane design. The results that were closely analyzed were the stall speed, balanced field length, and ferry range, which were then compared to the requirements specified by the RFP. A table of these results can be seen below, in Table 5.2-1.

Table 5.2-1: Results from the 12 Iterations

Iteration	AR	Engine	MTOW	Stall Speed (kts)	BFL (ft.)	Ferry Range (nm)
1	8	CF34-8C5	89,676	86.33	5300	2828
2	8	CF34-8E	89,826	86.41	4980	2820
3	8	CF34-10A	90,036	86.51	4680	2808
4	8	CF34-10E	90,246	86.61	4500	2796
5	10	CF34-8C5	89,920	86.83	5450	2883
6	10	CF34-8E	90,070	86.90	5480	2874
7	10	CF34-10A	90,280	87.00	5400	2862
8	10	CF34-10E	90,490	87.11	5310	2850

9	12	CF34-8C5	90,410	87.05	5800	2805
10	12	CF34-8E	90,560	87.12	5430	2796
11	12	CF34-10A	90,770	87.22	5250	2785
12	12	CF34-10E	90,980	87.32	5100	2773

It can be seen that the stall speed requirement of 90 knots is met for all 12 iterations without significantly exceeding it. The ferry range requirement of 2,500 nm is also met for all 12 iterations. However, the balanced field length requirement of 5,000 ft. is only met for a few iterations. The carpet plots in Figures 5.2-1 and 5.2-2 better illustrate this phenomenon.

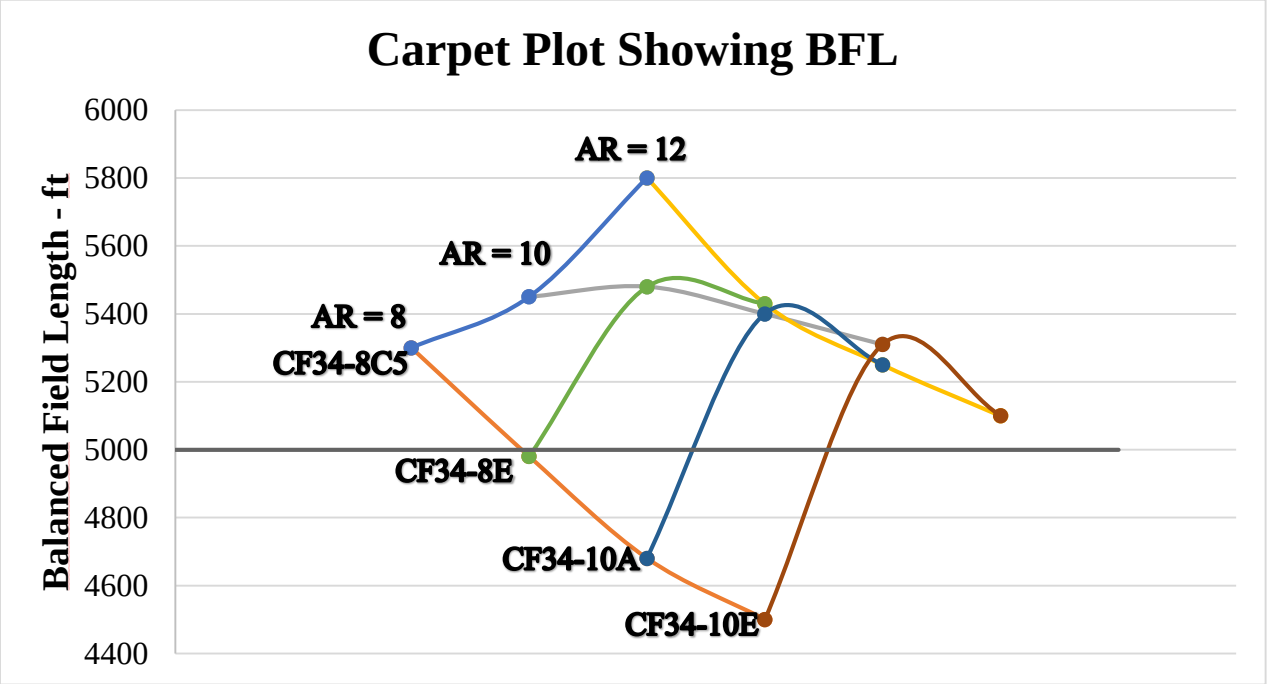

Figure 5.2-1: Carpet Plot showing Balanced Field Length data

The carpet plot in Figure 5.2-1 was used, in conjunction with the BFL requirement of 5,000 ft, to create a new carpet plot, shown in Figure 5.2-2. This new carpet plot shows this data plotted

against the maximum takeoff weight, which helped determine the optimal combination between aspect ratio and engine.

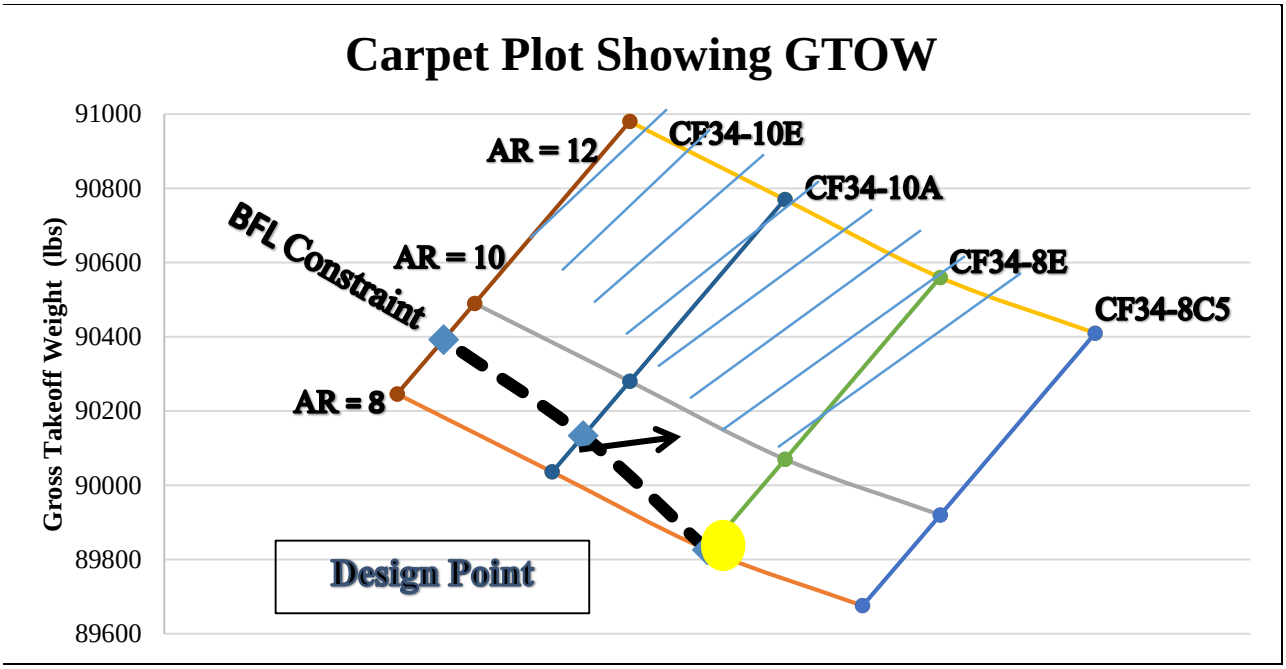

Figure 5.2-2: Carpet Plot showing Maximum Takeoff Weight

The BFL constraint, shown with a black dashed line, is created by using the BFL requirement and where it intersects with the curves in Figure 5.2-1. The area below the BFL constraint line is the desired area. Therefore, the selected design point is an AR of 8 and the CF34-8E engine, since it results in the lowest GTOW, while still meeting the BFL requirement. This point also signifies the combination of AR and engine that meets the BFL requirement without greatly exceeding it.

6. Wing Selection

As mentioned in section 5.0, the optimal aspect ratio for the wing was determined to be 8. Using the 89,076 lb. MTOW of the aircraft and the previously determined wing loading of 47.69 psf, the area of the wing was calculated to be 1868 ft^2. (Note: a detailed discussion of the MTOW calculation is discussed in Section 11). The quarter chord was chosen to have a 0° sweep since the aircraft will be flying at subsonic speeds where fluid compressibility is negligible and there are no shock waves. For determining the taper ratio, further research was done by looking at existing aircraft' trend data. Raymer [5] mentions that "most wings of low sweep have a taper ratio of about 0.4-0.5" (Raymer [5], 55). Also, in Schaufele [3]'s Fig. 4-9, it is stated that taper ratios range from 0.4 to 0.2 for jet transports. Hence, a taper ratio of 0.4 was chosen, yielding a nearly elliptical lift distribution, which can be seen in Figure 7.6-1.

6.1 Wing Planform

The wing area, aspect ratio, taper ratio, and quarter chord sweep were used to determine the wing geometry, which can be seen in Figure 6.1-1. The wing has a span of 122.24 ft., a root chord of 21.84 ft. and a tip chord of 8.73 ft., resulting in a mean aerodynamic chord (MAC) of 16.22 ft., which is located 26.19 ft. from the center of the wing. The important wing parameters and dimensions are listed in Table 6.1-1.

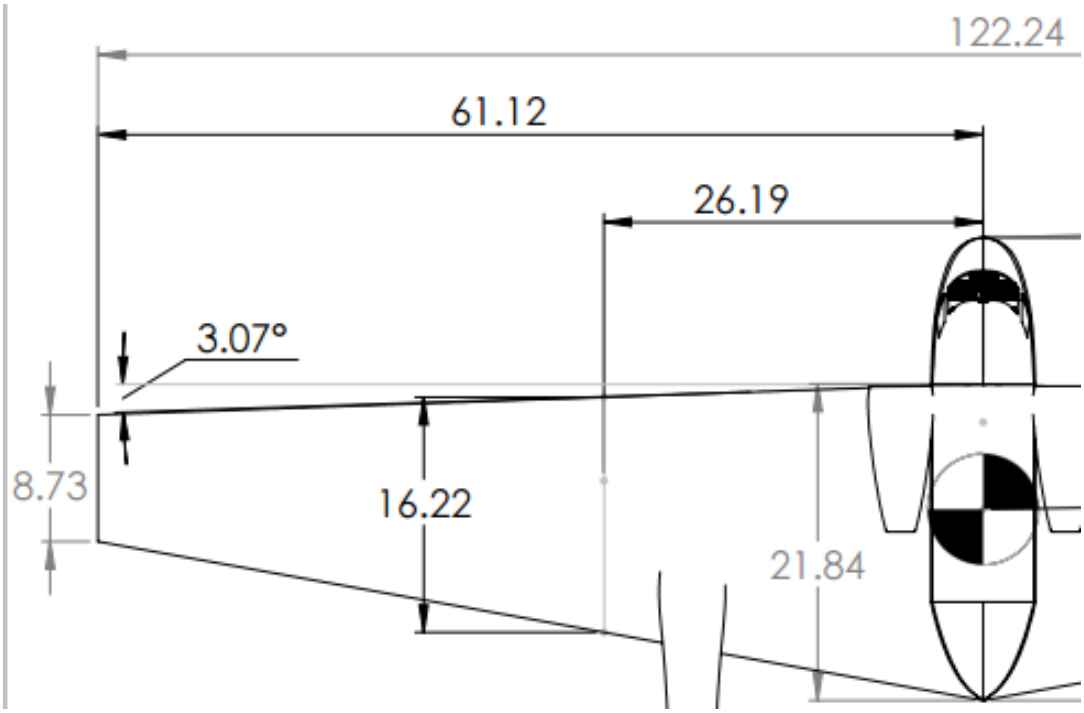

Figure 6.1-1: Semi span planform of the wing (all dimensions are in feet)

Table 6.1-1: Important wing parameters and dimensions

AR	8
Span	122.4 ft
MAC	16.22 ft
Root Chord	21.84 ft
Tip Chord	8.73 ft
Taper Ratio	0.4
Sweep	0˚

6.2 Airfoil Selection

When selecting the airfoil for the LAT - 1, NACA airfoils of 8% to 15% thickness ratio were investigated using wind tunnel data from the Theory of Wing Sections. Four aerodynamic characteristics were used to rate each airfoil. These characteristics were maximum lift coefficient, C_l at zero geometric angle of attack, drag coefficient at zero lift, and drag coefficient at maximum lift coefficient. These characteristics were chosen to select an airfoil with a large C_{LMax} and higher lift to drag ratios for the aircraft. From the results in Table 6.2-1, it is shown that the NACA 63_2-415 is the only airfoil to make top four in each category of the 10 airfoils considered. This airfoil is used as a root airfoil. The tip airfoil chosen is the NACA 63-209, which was chosen because it was the highest scoring airfoil available with a thickness ratio of less than 10%.

Table 6.2-1: Airfoil characteristics of top preforming airfoils in $C_{l\,max}$, C_{l0}, C_{d0}, and C_d (C_{lMax}). With Re = 9 million

Characteristic	Third Ranked	Third Ranked	Second Ranked	Top Performer
Airfoil	4415	63_2-415	23015	23012
$C_{l\,max}$	1.64	1.67	1.72	1.8
Airfoil	2412	63_2-415	4412	4415
C_{l0}	0.25	0.3	0.4	0.45
Airfoil	63_2-415	2408	63-209	63_2-215
C_{d0}	0.006	0.0058	0.0052	0.0048
Airfoil	63_2-215	63-209	63_1-212	63_2-415
$C_d(C_{l\,Max})$	0.0152	0.0128	0.0128	0.0122

These airfoils are particularly advantageous because of the drag buckets associated with these airfoils. These airfoils have minimum drag with section lift coefficients greater than 0. The NACA 63_2-415 has a minimum drag between $C_l = 0.2$ and 0.6. The NACA 63-209 has its minimum drag between $C_l = 0.1$ and 0.3. This characteristic is favorable, because small decreases in drag

can cause larger increases in Lift to drag ratios. The drag polars for each of the airfoils are plotted in Figure 6.2-1.

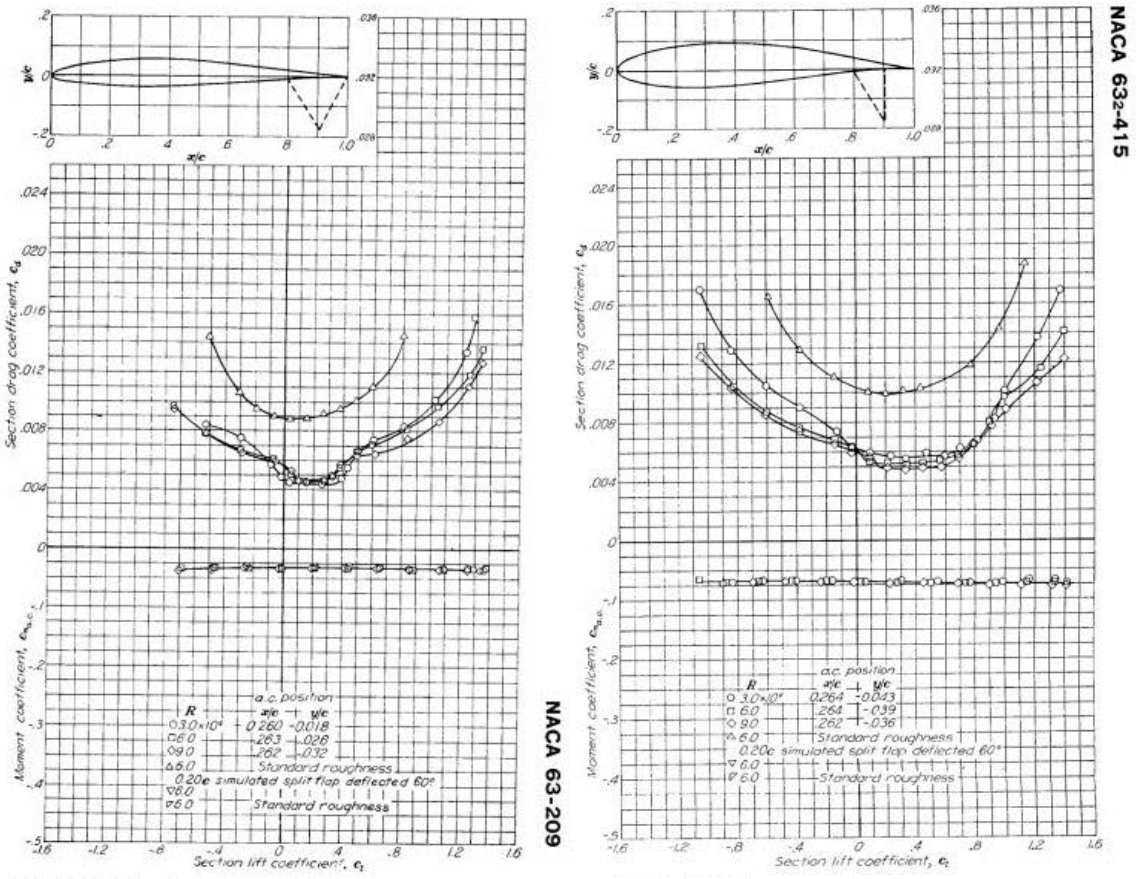

Figure 6.2-1: Drag Polars for the NACA 63_2-415 and NACA 63-209 airfoils from Abbott and Von Doenhoff's Theory of Wing Sections [11]

7. Aerodynamic Analysis

7.1 Aerodynamic Lift

7.1.1 Low Speed Lift Curves

Low speed lift curves were analyzed using methods described in Elements of Aircraft Preliminary Design by Schaufele [3] with comparisons to LinAir desktop aeronautics, which uses vortex lattice method and inputted airfoil data, found in Abbot and Von Doenhoff's Theory of Wing Sections [11]. To do so, the lift curve slope, airplane C_{Lmax}, and lift coefficient at zero angle of attack must be found. To begin analysis, the aircraft lift curve slope and maximum coefficient of lift for the wing in clean configuration are found. By using the wing aspect ratio of 8 and a quarter chord wing sweep of 0°, a lift curve slope of the wing is found to be $\partial C_L/\partial\alpha = 0.084$. This was verified using LinAir which returned a lift curve slope of $\partial C_L/\partial\alpha = 0.082$. To account for lift contributions from the rest of the aircraft, an additional 8% was added to the wing slope for an airplane lift curve slope of $\partial C_L/\partial\alpha = 0.088$. Using the trend for C_{lMax} with airfoil thickness and the airplane C_{Lmax} to airfoil C_{lMax} ratios an expected C_{Lmax} of 1.47 was found. Using airfoil data inputs for the selected airfoils in LinAir, a clean C_{Lmax} of 1.49 was found. The lift coefficient at zero angle of attack was found in LinAir to be $C_{L0} = 0.36$. Effects of trailing edge flaps for takeoff and landing configurations was characterized by changing the zero lift angle of attack. The Lift curve slopes for each case are shown in Figure 7.1-1 and C_{Lmax} for each configuration are listed in Table 7.1-1.

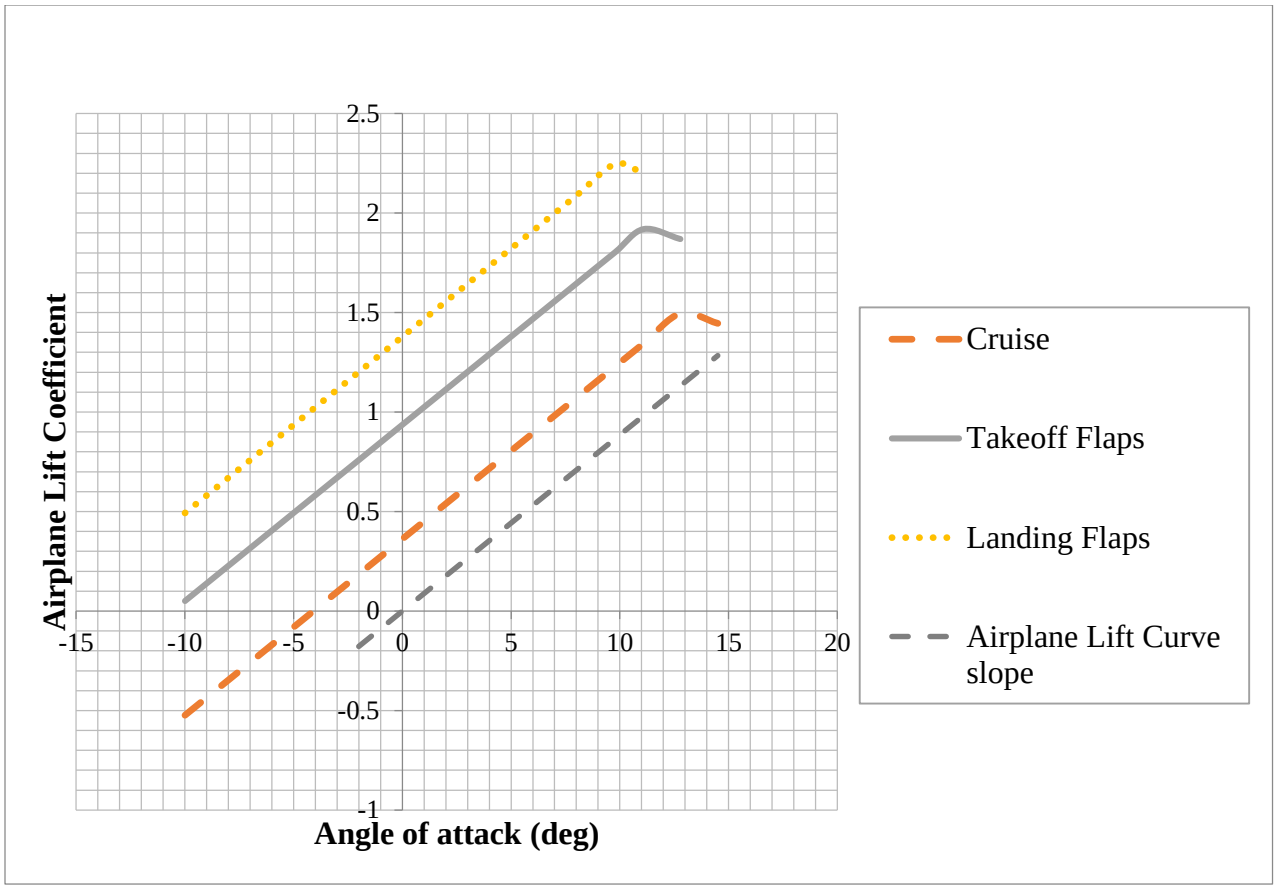

Figure 7.1.1-1: Low speed lift curves at landing, takeoff, and clean conditions

The flaps considered use a flap chord to wing chord ratio of $c_f/c = 0.25$ and a ratio of effected wing area to total wing area of $S_{WF}/S_W = 0.64$. For takeoff and landing configurations a 25° flap deflection and 50° flap deflection are used, respectively. These values were used to reach a maximum lift coefficient at a landing flap configuration of 2.25 in order to meet the required stall characteristics. The maximum lift coefficient at negative angle of attack was found to be -1.40. These C_{Lmax} values were used to determine the 1 g stall speeds for both positive and negative angles of attack, and can be seen in Figure 12-1.

Table 7.1.1-1: C_{Lmax} at various configurations

Flight Configuration	C_{Lmax}
Clean	1.49
Takeoff	1.92
Landing	2.25

7.1.2 Spanwise Lift Distribution

Spanwise Load Distribution was calculated across the wing using LinAir Desktop Aeronautics. The spanwise lift distribution was calculated at zero angle of attack and at the angle of attack at which C_{LMax} occurs. These lift distributions are used in the total spanwise load distribution in structural analysis of the wings. The section lift coefficient for cruise configuration is normalized by the total lift coefficient in Figure 7.1.2-1.

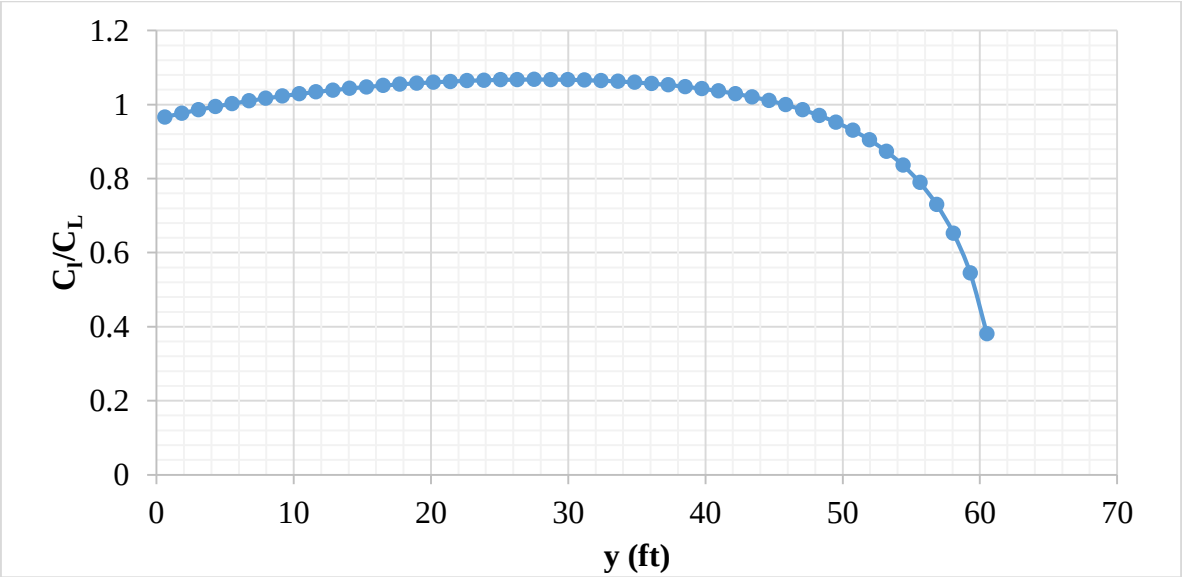

Figure 7.1.2-1: Normalized section lift coefficient across the semi span of the wing

7.2 Drag Build-Up

The total drag is typically made up of induced, parasitic, and compressibility drag. It is noted that the mission of this aircraft does not include high speed flights at which compressibility drag would be an issue. However, the drag at high subsonic Mach numbers was still obtained and used to create the operational envelope of the aircraft, which is described in more detail in Section 10.3.

7.2.1 Parasite Drag

Parasite drag was calculated using the method specified in Schaufele's Elements of Aircraft Preliminary Design [3]. In doing so, all parts of the aircraft that produce parasitic drag were considered. This includes the wing, horizontal tail, vertical tail, fuselage, engine nacelles and pylons, booms, flap hinge covers, as well as miscellaneous objects such as antennae, pitot tubes, etc. The parasite drag for each element was individually calculated using equation 7.2.2-1, then totaled to find the parasite drag for the airplane.

$$C_{Dp} = f/S_{ref} \qquad \textbf{Equation 7.2.1-1}$$

where f is the equivalent parasite drag area and is defined as

$$f = K\, C_f\, S_{wet} \qquad \textbf{Equation 7.2.1-2}$$

where K is the form factor for the individual element in consideration, C_f is the skin friction drag that the element produces, and S_{wet} is the total wetted area of that element. Since the airplane will be operating at high Reynold's numbers, the flow along the surfaces are assumed to be fully turbulent. Equation 7.2.2-3 is used to calculate the skin friction drag coefficient in turbulent flow.

$$C_f = 0.455/(\log_{10} Re)^{2.58} \qquad \textbf{Equation 7.2.1-3}$$

A build-up of the parasite drag of the airplane can be seen in Figure 7.2.2-1 and Table 7.2.2-1. The total parasite drag at cruise speed is found to be 0.0154. The wing has the largest contribution to this parasitic drag with a 54.58% contribution.

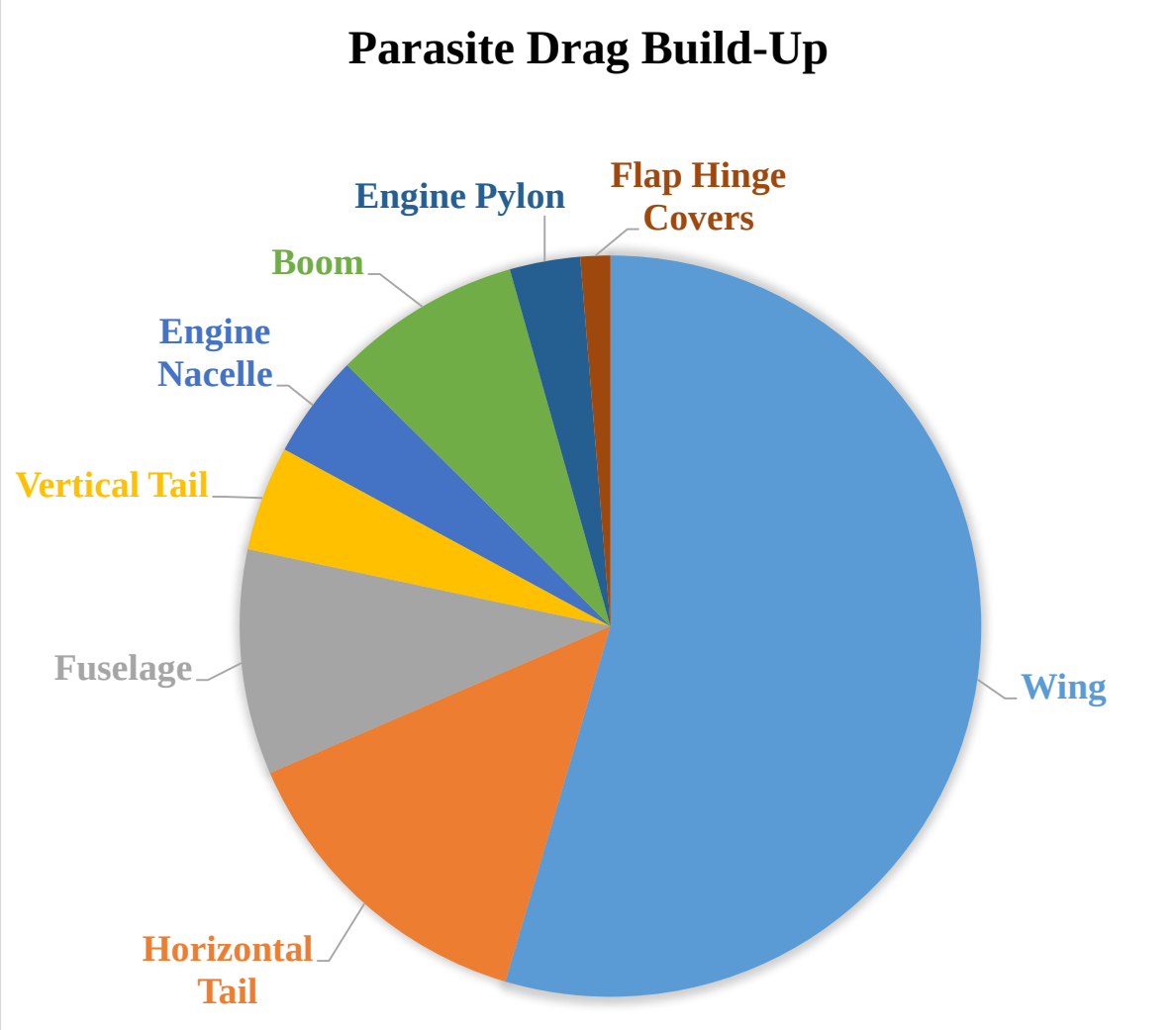

Figure 7.2.1-1: Parasite drag build-up at cruise speed

Table 7.2.1-1 Parasite drag build-up at cruise speed

	C_{Dp}	Contribution
Wing	0.00629	54.58%
Horizontal Tail	0.00161	13.94%
Fuselage	0.00113	9.82%
Vertical Tail	0.00053	4.58%
Engine Nacelle	0.00052	4.52%
Boom	0.00094	8.19%
Engine Pylon	0.00035	3.07%
Flap Hinge Covers	0.00015	1.30%
Total	**0.01541**	100.00%

7.2.2 Compressibility Drag

As mentioned before, although the aircraft will not be operating at high subsonic speeds where compressibility drag effects occur, the drag calculations were still done for these high speeds in order to construct the operational envelope. Schaufele [3]'s Fig. 4-8 was used to find the drag divergence Mach numbers which were used, in conjunction with Schaufele [3]'s Fig. 12-10, to obtain the compressibility drag.

7.2.3 Induced Drag

Induced drag was calculated, in the typical manner, using Oswald's efficiency factor. Oswald's efficiency factor was calculated using equation 12.49 from Raymer's Aircraft Design [5]: A Conceptual approach, and by inputting airfoil drag characteristics into LinAir desktop aeronautics. The equation from Raymer [5] returned an efficiency factor of e = 0.81. This equation is restated in eq. 7.2.1-1.

$$e = 1.78(1 - 0.045A^{0.68}) - 0.64 \qquad \textbf{Equation 7.2.3-1}$$

LinAir uses parabolic fit terms of airfoil data to characterize the airfoil. The data from Theory of Wing Sections was logged and fit with a parabolic curve. LinAir returned an efficiency factor of e = 0.85. These quadratic equations have a linear term, which indicates that the minimums of the parabola are not at the zero lift line, but at a position of positive C_L. For this wing, the C_L of minimum drag was found to be 0.04. Although this number is small compared to the minimum drag lift coefficient in airfoil theory, the leftward shift of the drag polar increases the maximum wing lift-to-drag ratio from 18.1 to 19.3 in cruise configuration.

7.2.4 Drag Polar

The aircraft's drag polar for various flap configurations is shown in Figure 7.2.4-1. This plot highlights the C_L of minimum drag for the aircraft.

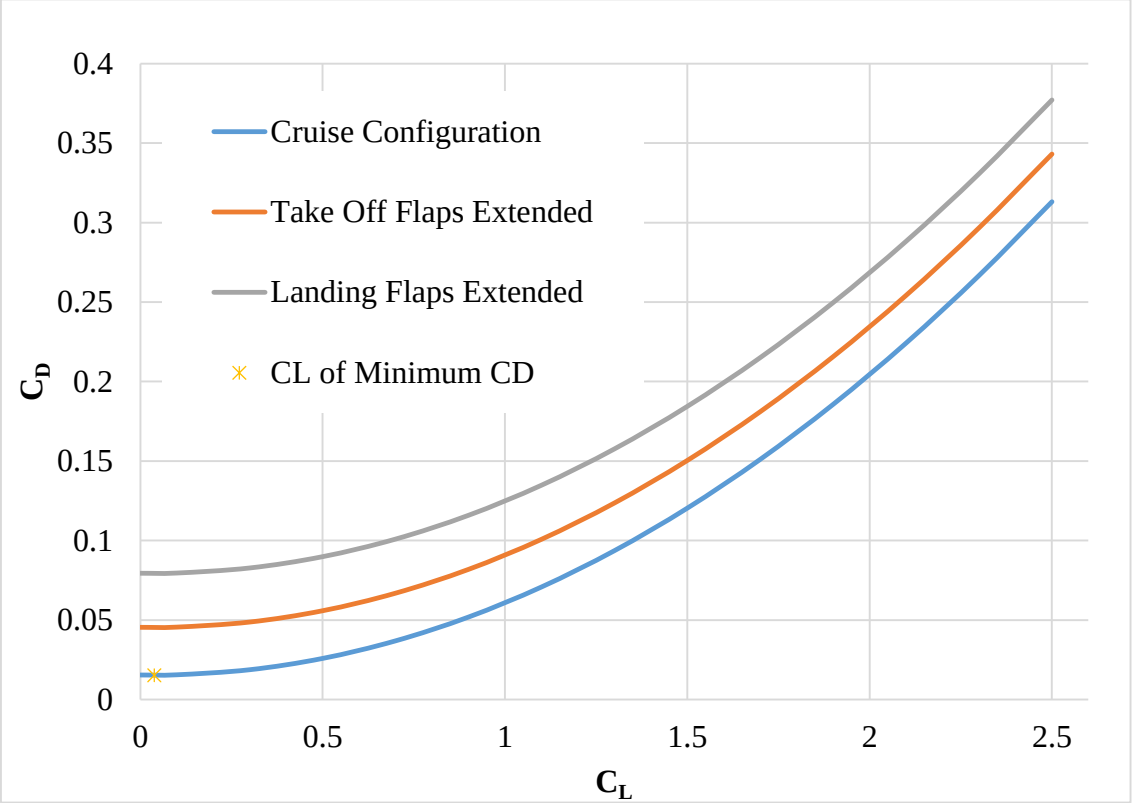

Figure 7.2.4-1: Drag polar curves for various flap extension configurations

7.2.5 Lift to Drag Ratios

The aircraft showed its best lift-to-drag ratios at lift coefficients of about 0.5. Since the aircraft does not approach its drag divergence Mach number at top speeds, compressibility has little affect, and our aircraft will have higher lift-to-drag ratios at higher velocities. Plots of lift to drag ratios are shown in Figure 7.2.5-1. These plots show maximum lift-to-drag ratios of 18.4, 18.9, and 19.3 at Mach numbers of 0.2, 0.3 and cruise, Mach 0.382, respectively.

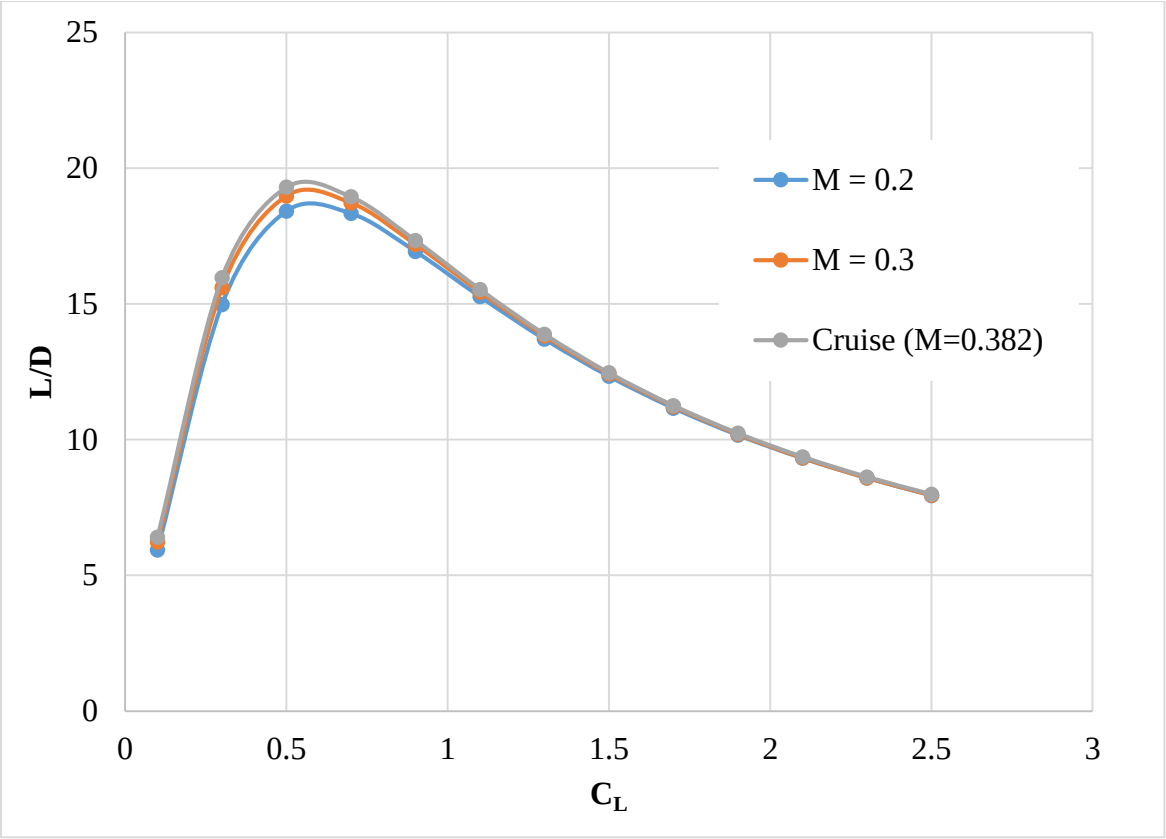

Figure 7.2.5-1: C_L vs L/D at Mach numbers of 0.2, 0.3 and 0.382

8. Stability & Control

Stability and control calculations drove the CG location relative to mean aerodynamic chord and tail volume coefficients of the aircraft design.

8.1 Horizontal Tail Sizing (Notch Chart)

During the early stages of this design study, the horizontal tail volume coefficients was assumed to be similar to those of other aircraft with similar mission and configurations. This early assumption was later replaced with a configuration specific volume coefficient found using a notch chart. This notch chart was generated based on the pitch control authority required in four different scenarios. These scenarios are:

1. Static margin with the CG at the aft most position
2. Landing with full flaps with the CG at the fore most position
3. Takeoff with the CG at the fore most position
4. Controlled flight through maximum CG travel

The resulting takeoff pitch, landing pitch, and static margin limits can then be plotted in terms of horizontal tail volume coefficient over CG location as a percentage of mean aerodynamic chord. A horizontal line with a width equal to the maximum CG travel can then be fitted down into the notch formed by the stability lines. The height of the line at the bottom of this notch indicates the minimum horizontal tail coefficient required to meet all of the above criteria.

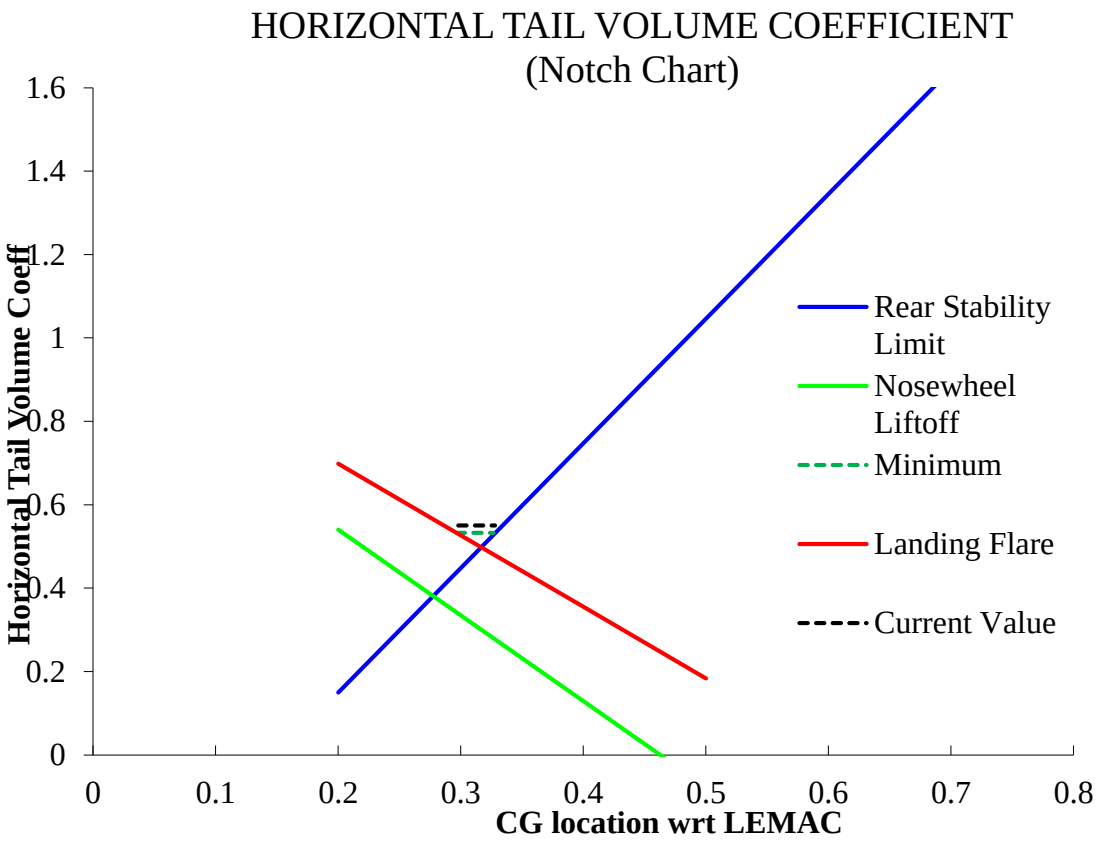

Figure 8.1-1: Notch Chart

The notch chart for our design calls for a minimum horizontal tail coefficient of 0.53, but to allow for some safety margin we choose a slightly higher volume coefficient of 0.55. Note that due to the very dense nature of the payload, we were able to keep the CG travel extremely short, allowing for a smaller horizontal tail volume coefficient than would otherwise be required.

Table 8.1-1: Important horizontal tail parameters and dimensions

Tail area	426 ft^2
Distance from CG to tail MAC	39.1 ft
Aspect ratio	4
Span	41.3 ft
Chord	10.3 ft
Taper ratio	1
Sweep	0°

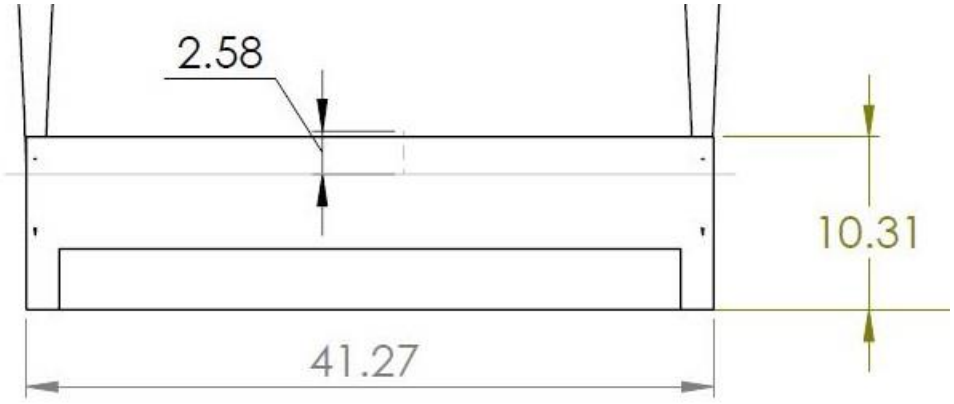

Figure 8.1-2: Horizontal tail planform

8.2 Vertical Tail Sizing (Minimum Control Speed)

Similar to the horizontal tail, the vertical tail was initially sized by assuming that our design would have a vertical tail volume coefficient similar to those of other aircraft with similar roles and configurations. As the design matured and a more accurate figure was required, minimum control speed was selected as the factor driving the size of the vertical tails. For maximum safety, we chose to exceed the FAA required minimum control speed of $1.13V_{stall}$ and simply make minimum control speed equal to stall speed.

To find the minimum tail size that achieves a minimum control speed equal to stall speed, first the adverse yaw moments were summed. Sources of this moment included the one operative engine producing its maximum rated thrust and the inoperative engine's windmill drag. This adverse moment must now be matched by a restorative moment equal in magnitude and opposite in direction. The source of this restorative moment would be the vertical tails with their rudders at maximum deflection.

The force produced by the tails is not as simply predicted as the thrust and windmill drag of the engines. This force is a function of the tail shape (height, chord, taper, airfoil, etc.), the rudder size and deflection angle, and the dynamic pressure at the desired speed (stall speed). The actual restorative moment is then this force multiplied by the length of the moment arm, which is the distance from the aft most CG location to the mean aerodynamic chord of the vertical tails.

Table 8.2-1: Important vertical tail parameters and dimensions

Tail area (total)	152 ft^2
Distance from CG to tail MAC	41.8 ft
Aspect ratio	1.3
Height	9.9 ft
Root chord	6.7 ft
Upper tip chord	7.6 ft
Upper taper ratio	.68
Upper sweep	23°
Lower tip chord	4.86
Lower taper ratio	.72
Lower sweep	27°
Rudder deflection angle	26°

All of these relations were analyzed using a Microsoft Excel sheet that could solve for zero overall moment by varying any of the tail parameters. After multiple iterations, a final tail size was selected that would be a good compromise between low weight, tip back angle, and buckling strength (for supporting the horizontal tail).

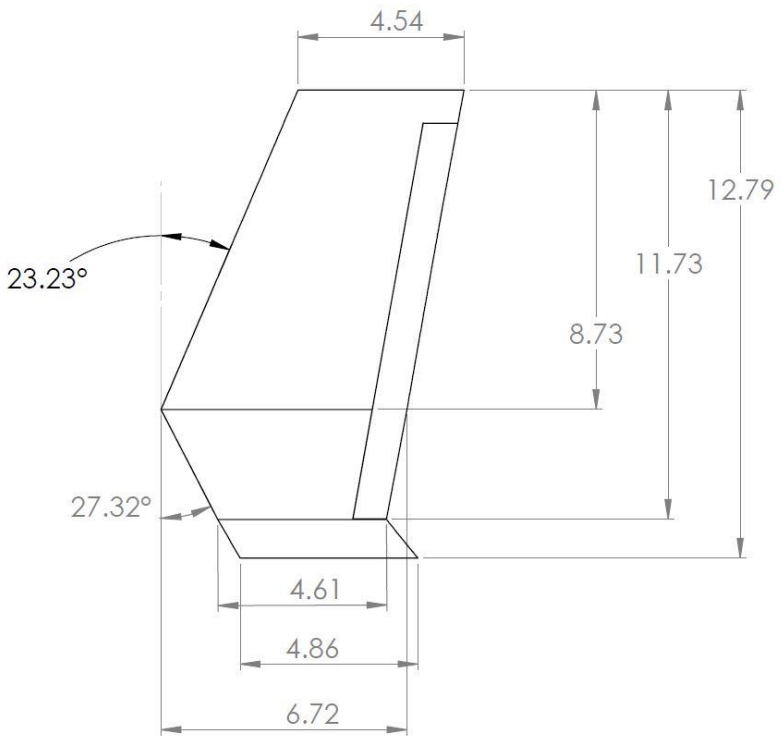

Figure 8.2-1: Vertical tail planform

8.3 Tail Configuration

While twin boom tail configurations are not commonly seen on modern aircraft the unique nature of the mission for which our aircraft is designed made it a compelling choice for a wide variety of reasons. High mounting the horizontal tail (for better efficiency) is easier since the horizontal tail is supported at two locations instead of just one. Having the supports at the ends also allows for a longer horizontal tail span and a larger elevator, allowing for increased pitch control authority.

Additionally, the biggest disadvantage of a twin boom design is actually an advantage for this particular mission. Twin boom aircraft tend to have very small pod-like fuselages, but since our design is only ever required to carry a dense liquid payload the small fuselage greatly reduces wasted space.

9. Aircraft Engine

9.1 Engine Selection

As per the RFP requirements, the engine selection was limited to either a turbofan, or turboprop engine. Due to the high thrust and/or propulsive force required to meet balanced field length requirements, a high bypass turbofan engine was selected. Selecting a turbofan type engine also allowed for flexibility of engine placement during the design process, in the event of a weight-balance change. With a MTOW of 89,000 lbs and a thrust-to-weight ratio of 0.44, the aircraft would need approximately 39,160 lb_f of thrust. The thrust-to-weight ratio shown above was selected mid-way through the design process based on the most constraining condition in the constraint diagram, in which the aircraft must achieve of balanced airfield length of no greater than 5,000 ft at an elevation of +5,000 ft with a +35 °F temperature offset.

Knowing that a turbofan engine would be utilized for the design, the team was able to select a grouping of engines that all could meet the total thrust requirement of 39,160 lb_f. With the information currently available in the public domain, the main parameters that were compared to narrow the engine selection was total static thrust (lb_f.), specific fuel consumption, and the thrust-to-weight ratio of the engine itself. The comparison of 5 different engines that are the most likely to successfully meet the required thrust is shown below in Table 9.1-1.

Table 9.1-1: Turbofan engine specifications

Manufacturer	Engine	Static Thrust (lbf)	TSFC lbm/hr/lbf	Dry Weight (lbs)	Engine Specific T/W (lbf/lb)
CFM	CFM56-7B20	20,600	0.36	5,216	3.95
GE	CF6-50A	49,000	0.389	8,731	5.6
GE	CF34-10A	20,360	0.38	3,800	5.36
IAE	V2522-A1	22,000	0.34	5,250	4.19
Ivchenko	D-436T1	16,800	0.378	3,090	5.43

Of the selected engines, at least three successfully fit the needs for the aircraft. Those engines are shown highlighted yellow, in Table 9.1-1. With a minimum thrust required of below 40,000 lb_f it was determined that designing the aircraft with two engines would be an appropriate solution. Not only does having two engines mitigate the risk of a loss-of-vehicle incident in a one-engine-inoperative condition, but also eases the selection process for an engine that produces approximately 20,000 lb_f of thrust. Given the aircraft thrust-to-weight estimation made previously from the constraint diagram, the General Electric CF34 line of engines could meet and exceed the thrust requirements, if installed as a pair of two.

The engine finally selected for this design is the General Electric CF34-8C, which produces a peak static thrust of 23,600 lb_f, and an estimated SFC of 0.38 lbm/hr/lbf at cruise. This engine successfully met the thrust requirements, but also allowed the aircraft to meet the balanced field length requirement, without excess thrust and engine weight, that would have been a hindrance on an empty aircraft during a ferrying mission. Emphasis was placed on the GE CF34 line of engines during the selection process due to the overall simplicity of engine maintenance in comparison to engines manufactured by other countries that produced a similar thrust output, as well as the familiarity that many civilian aviation mechanics already have with the operation and maintenance of the CF34 engines. This then avoids an extra training expenditure for the customer's selected maintenance crews. In addition, the CF34 line exhibits a superior specific thrust-to-weight ratio for the engine itself, in comparison to engines manufactured by Ivchenko and CFM.

9.2 Engine Mapping

The GE CF34-8C engine mapping is shown below in Figure 9.2-1, Courtesy of Eric Schrock [1]. The conditions of the engine mapping correlate to the takeoff conditions outlined by

the RFP; +5,000 ft. altitude, +35°F hot weather conditions, with 5% bleed air. The points along the curve were selected correlate directly to acceleration stage of balanced field length calculations.

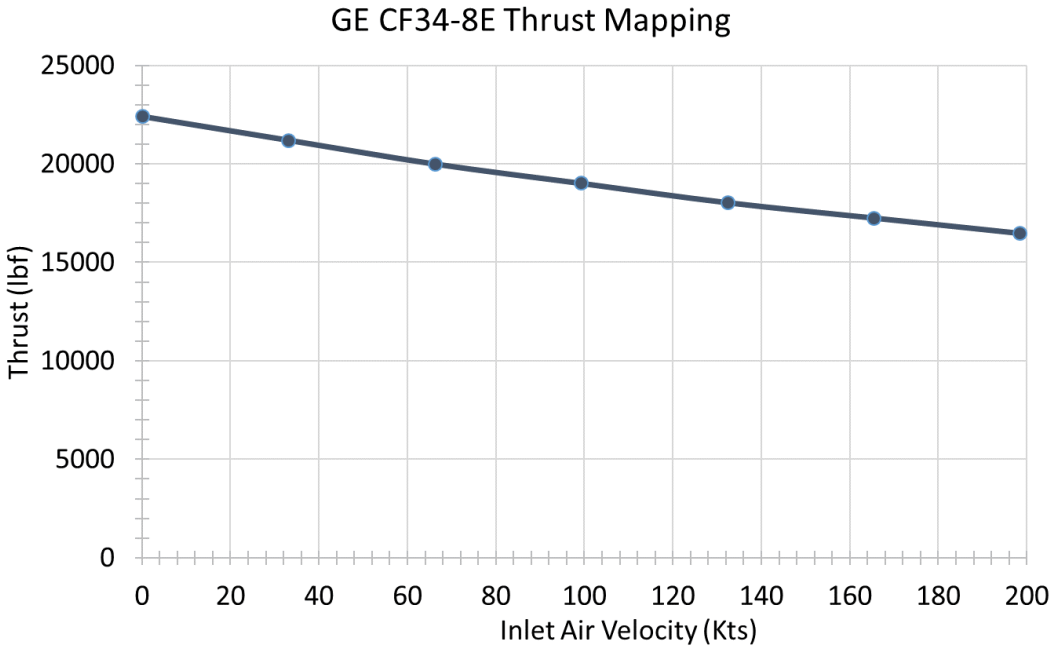

Figure 9.2-1: CF34-8E thrust mapping

9.3 Engine Placement

Engine placement for our aircraft quickly became a variable when calculating the weight-balance of the aircraft, and one-engine-inoperative conditions. To avoid an overly large vertical tail, the goal was to place the engines as close to each other as possible, thus limiting the yawing moment created by having an engine out. One of the best ways to prevent this yawing moment is to place the engines on the top surface of the wing, thus not being constrained by the width of the fuselage.

By placing the engines on the top surface of the wing, our aircraft also gains the ability to land on unimproved runways and landing strips. While the RFP does not explicitly state that the

runway is, or is not an improved surface, having the ability to land and takeoff on a dirt runway and not ingesting dirt and foreign object debris (FOD) allows the aircraft to be significantly more flexible with where it operates out of.

One of the main risks associated with mounting the engines on the top surface of the wing, is their proximity to both the fuel tank, and the main wing spars. In the event of an uncontained rotor burst, the rotors can tear through the fuel tank and cause fire, and structural damage to the wing spars. To mitigate structural damage, the engine nacelle will have a Kevlar shield around the entre engine, as well as a shield to protect the spars and the fuel tanks. To further prevent fire, the fuel tank will be made with a self-sealing bladder to prevent and limit the likelihood of fuel leaks if the tank becomes punctured these self-sealing bladders already see action in the auto-racing and small UAV industry with the company Aero Tech Laboratories, or ATL. These bladders are designed to deform and take heavy impacts before a puncture occurs, and in the event of a puncture the bladder is elastic enough to seal the tear on its own. By including these fuel bladders, and protective shields under the engine, any risk associated with mounting the engines on the top surface of the wing is mitigated.

10. Performance Analysis

10.1 Payload-Range Calculation

The starting point for the payload range calculations was the 45,000 lbs. of retardant with no fuel which resulted in a range of 0 nm. The aircraft needs to perform a 200 nm radius mission to drop 45,000 lbs. of retardant on the fire to prevent it from spreading. Also, the aircraft needs to have enough fuel to perform a ferry range mission of 2,500 nm. For this mission, Ember Aviation decided that LAT-1 will be flying empty (with no payload) because there is really no necessity to fly this distance with a heavy aircraft. With this in mind, the initial range calculations were obtained by using the Breguet Range Equation. Since we have 2 different types of missions, the mission where the aircraft drops the retardant will be flying at its maximum takeoff weight (MTOW) of 89,076 lbs. and to perform the ferry range mission, it will fly empty (no payload) with a MTOW of 44,076 lbs.

To have a more detailed analysis of the fuel burned by the aircraft and range obtained with that fuel, the MTOW of the aircraft changed scenario by scenario. For instance, when performing the drop mission, the aircraft took off with a MTOW of 89,076 lbs. and cruised to the fire site for a total of 200 nm. Once the fuel needed for this step was obtained, it was subtracted from the MTOW along with the subtraction of the payload (no more payload when flying back to base). Once the fuel was calculated with no payload, and the subtraction of the fuel burned when flying to the fire site, this amount of fuel was also subtracted. Once this fuel to fly back to base was subtracted, we then added 45,000 lbs. of payload once again to the new MTOW (added payload weight because of refilling). Again, this process was done a total of 4 times because the RFP assumed to have the aircraft perform a total of 4 sorties to achieve a minimum time to establish a

fire line. The results of the complete payload range calculations are compiled in Table 10.1-1 and a payload range curve can be seen in Figure 10.1-1.

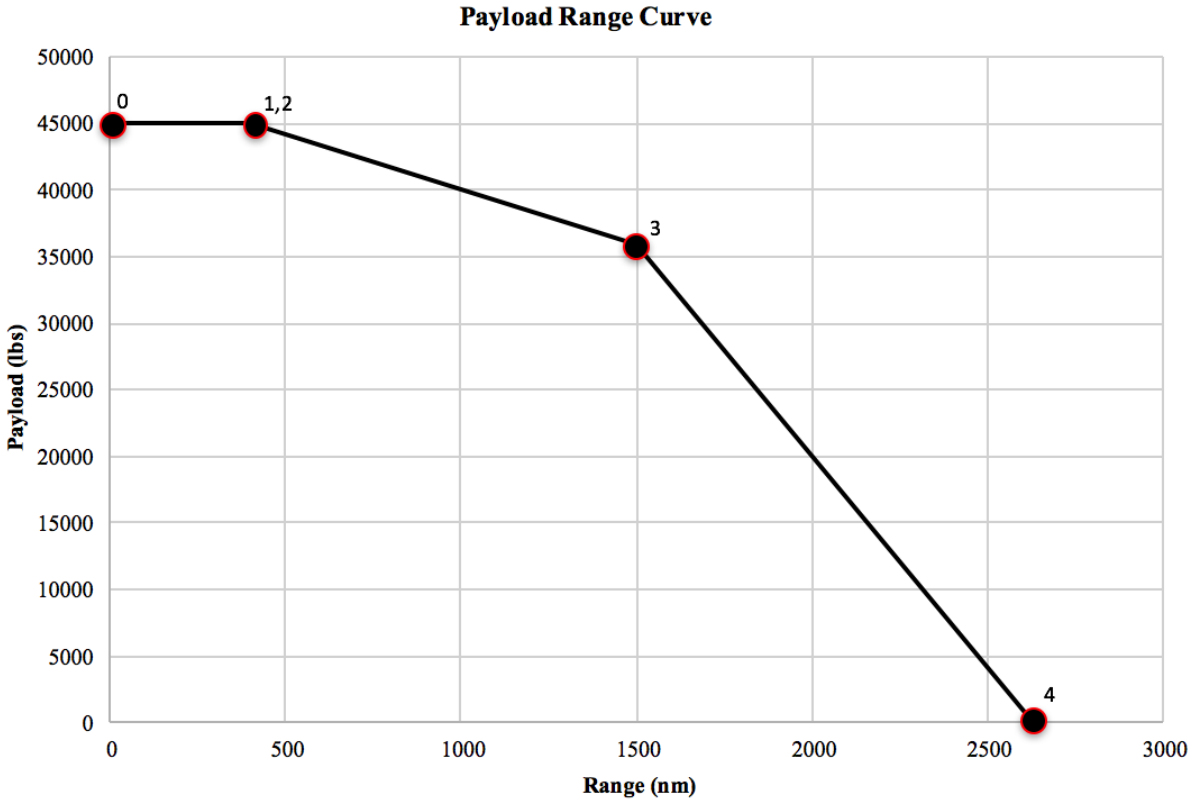

Figure 10.1-1: Payload range curve

Table 10.1-1: Payload, Fuel, and Range Calculated

Point	Payload (lbs.)	Fuel (lbs.)	Range (nm)
0	45,000	0	0
1	45,000	2,293	400
2	45,000	3,134	400
3	31,516	10,843	1,500
4	0	10,843	2,643

It is important to note that point 0 simply illustrates the aircraft with full no fuel, and full payload. Point 1 is when the aircraft performs the drop mission; furthermore, it only represents 1 sortie and for this sortie a total of 2,293 lbs. of fuel is needed. As previously explained in the paragraph before, the calculations were done for 4 sorties and it was concluded that the aircraft needs a total of 8,703 lbs. of fuel to establish a fire line. Point 2 of the graph represent the fuel needed for a mission where no retardant was dropped. This was taken into consideration because it is what yielded the heaviest MTOW for the design. For this mission with no drop, it was calculated that the aircraft needs a fuel of 3,134 lbs. Notice that there is more fuel required for this mission than that when the aircraft drops the payload because in this case we are returning to base with a full payload instead of empty. Point 3 illustrates the amount of payload the aircraft can carry if the fire site is in fact more than 200 nm from the base. It resulted in the aircraft to be able to carry 31,516 lbs. of payload with full fuel of 10,843 lbs. to travel a distance of 1,500 nm. Finally, point 4 represents the range that LAT-1 can travel on full fuel tanks and no payload. With full fuel tanks (10,843 lbs.) and no payload, LAT-1 can travel a total of 2,643 nm. This distance with no doubt meets the requirement of the RFP of having the ability to perform a ferry range of 2,500 nm. Also, the distance that the aircraft can travel on full payload and full fuel resulted in 1,328 nm.

10.2 Takeoff, Landing, and Balanced Field Lengths

The primary driving variable when calculating balanced field length for our aircraft was the weight of the airframe. Given the relatively moderate thrust requirement for the aircraft, selecting a larger engine always remained an option. Despite this, the goal was to optimize both the aspect ratio of the wing, and the engine size, weight, and thrust requirements, from balanced field length calculations. All calculations were performed at +5,000 ft. altitude, +35°F hot weather

conditions. If the aircraft was successful at meeting the balanced field length requirement of 5,000 ft. at this altitude and temperature offset, then it also meets the requirement at Standard Sea Level conditions. All one-engine-inoperative calculations were performed with one functioning engine only.

Balanced airfield length was outlined in Fundamentals of Aircraft and Airship Design [2], however all formulas and calculations were referenced from Chapter 16 of The Elements of Aircraft Preliminary Design [3]. Calculations of balanced field length were performed for 16 total conditions: four different aspect ratios, and four different engine thrusts. The resulting balanced field lengths are summarized below.

Table 10.2-1: Balanced Field Lengths for possible combinations

	Balanced Field Length (ft.)			
Aspect Ratio	**CF34-8C5**	**CF34-8E**	**CF34-10A**	**CF34-10E**
6	5,950	6,300	6,000	5,400
8	5,300	4,980	4,680	4,500
10	5,450	5,480	5,400	5,250
12	5,800	5,430	5,570	5,100

Given the above balanced field lengths, only three conditions met the 5,000 ft. requirement, all of which occurred with a wing aspect ratio of 8. Following are the balanced field length figures for the three successful configurations. Figure 10.2-1 utilizes the CF34-8E engine, Figure 10.2-2 utilizes the CF34-10A engine, and Figure 10.2-3 utilizes the CF34-10E engine. All calculations were performed assuming a 5,000 ft. altitude offset from sea level, and "hot day" conditions. These figures indicate both the calculated balanced field length, and the failure recognition speed, V_1.

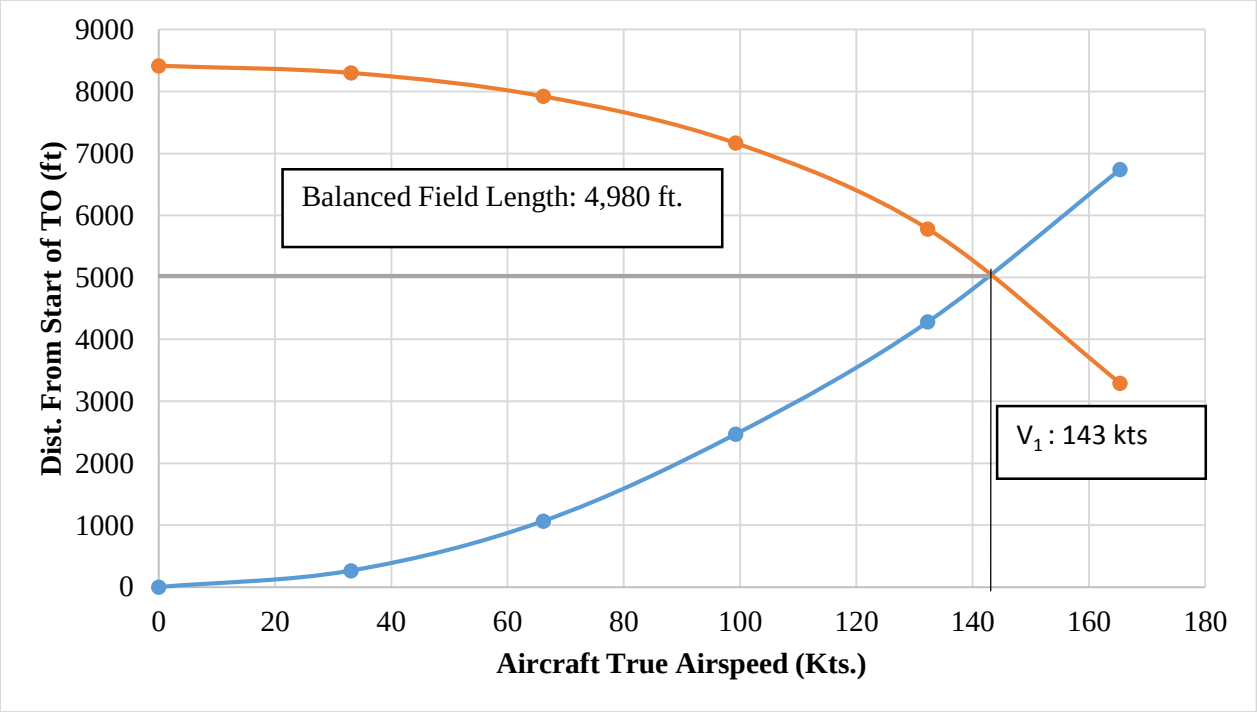

Figure 10.2-1: Balanced Field Length, CF34-8E

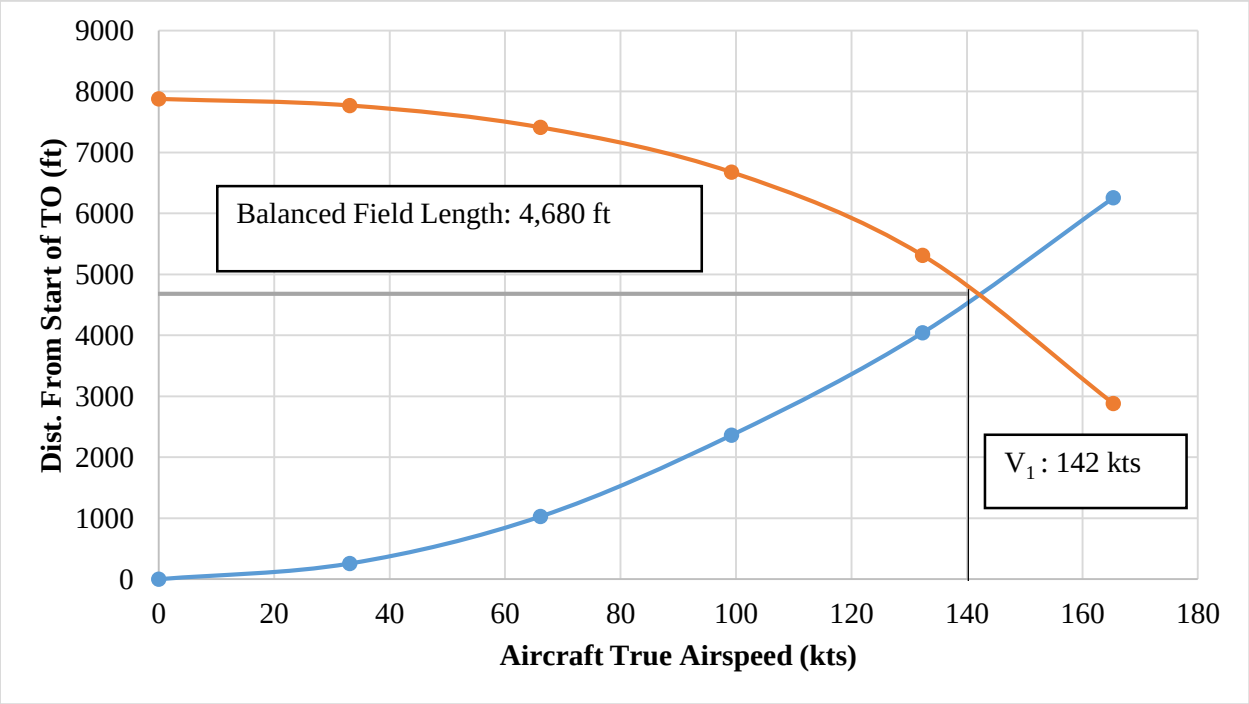

Figure 10.2-2: Balanced Field Length, CF34-10A

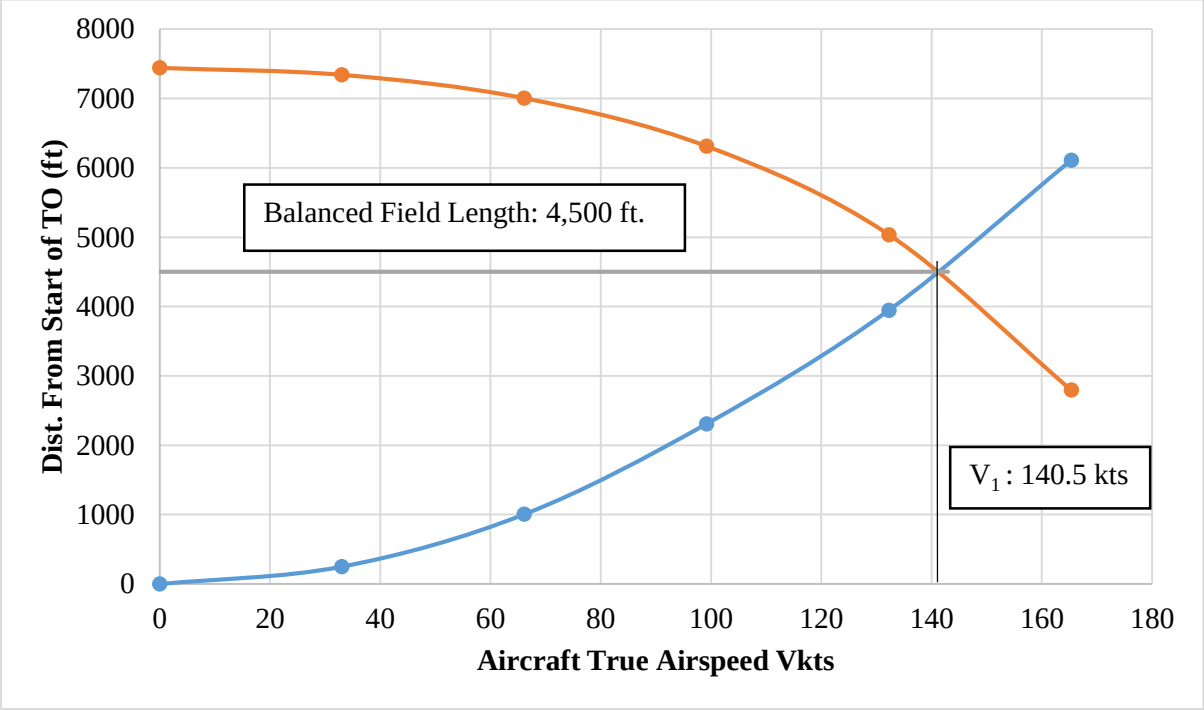

Figure 10.2-3: Balanced Field Length, CF34-10E

Figure 10.2-2 and 10.2-3 indicate that the thrust produced by the -10A, and -10E variants of the CF34 engine produce excess thrust, indicating the use of the marginally smaller -8E variant. This engine produces less thrust, exhibits a nominally better TSFC, and a lower engine weight than the other two variants, while still meeting the 5,000 ft. balanced field length requirement.

10.3 Operational Envelope

All aircraft are constrained to operate with altitude – airspeed boundary call the operational enveloped. An operational enveloped for the LAT-1 was created to show the boundaries that the aircraft is able to handle during flight. The operational enveloped described on a plot of pressure altitude versus true speed and consists three boundaries: minimum speed/stall speed boundary, minimum rate of climb/absolute ceiling boundary, and maximum speed/thrust equals drag

boundary. The boundaries were created using a method shown in Schaufele [3]'s design book. In Figure 10.3-1, stall speed, drop speed, and dash speed are inside the enveloped which shows that the LAT-1 meets the requirements in the RFP.

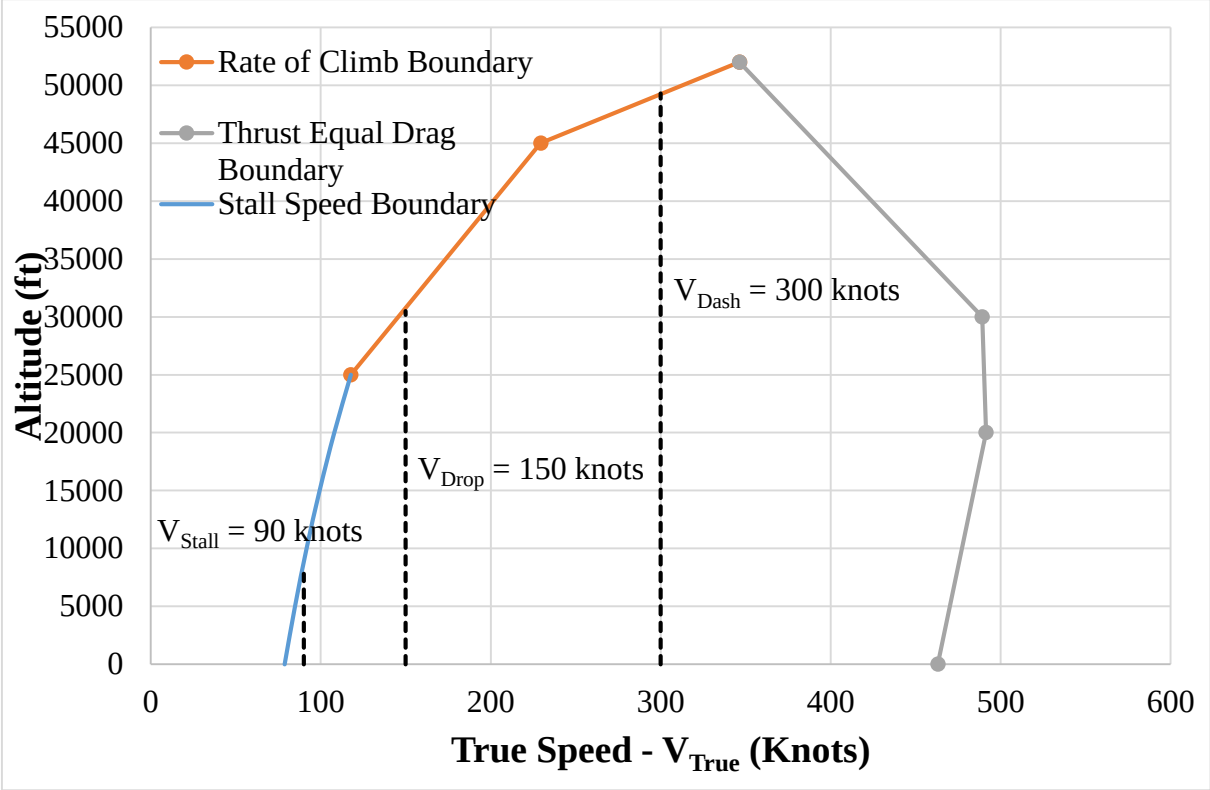

Figure 10.3-1: Operational envelope of the LAT-1

11. Weight Breakdown

After the preliminary 3-view layout drawing and the aircraft aerodynamic are completed, detail weight breakdown of the LAT-1 can be performed as well as the balance calculation. These calculations are important since the weight and center gravity location of each component help to assure the wing location on the fuselage is correct. This section shows the methods were used to determine the detail weight breakdown and center of gravity location of the LAT-1.

First, four component weight breakdowns were calculated: using methods from aircraft design books by Daniel Raymer [5], Nicolai & Carichner's [2], and Dr. Jan Roskam (General Dynamic method and Torrenbeek method). There four methods were compared with weight percentages from Schaufele [3]'s aircraft design book. Finally, the average percentage of four methods was used to obtain the weight breakdown of the LAT-1. The resulting dry weight breakdown is shown in Table 11-1

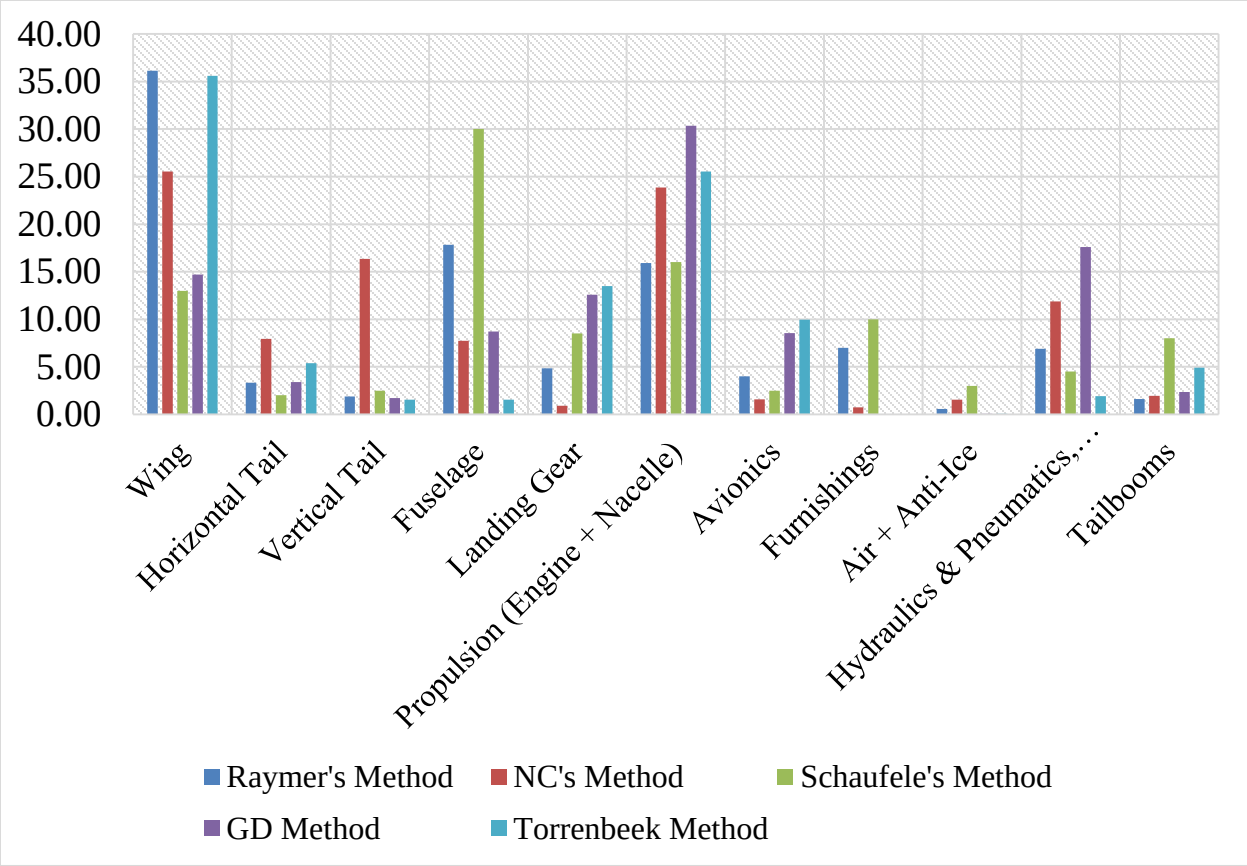

Figure 11-1: Percentage weight breakdown comparison between different methods

Table 11-1: Dry weight breakdown of the LAT-1

Component	Weight %	Weight (lbs)
Wing	25	7,878
Horizontal Tails	4	1,390
Vertical Tails	5	1,512
Fuselage	13	4,149
Landing Gear	8	2,541
Propulsion (Engine + Nacelle)	22	7,039
Avionics	5	1,676
Furnishings	3	1,118
Air + Anti-Ice	1	331
Crew	2	500
Hydraulics & Pneumatics, Electrical, APU	8	2,697
Tail booms	4	1,186
Total	100	32,016

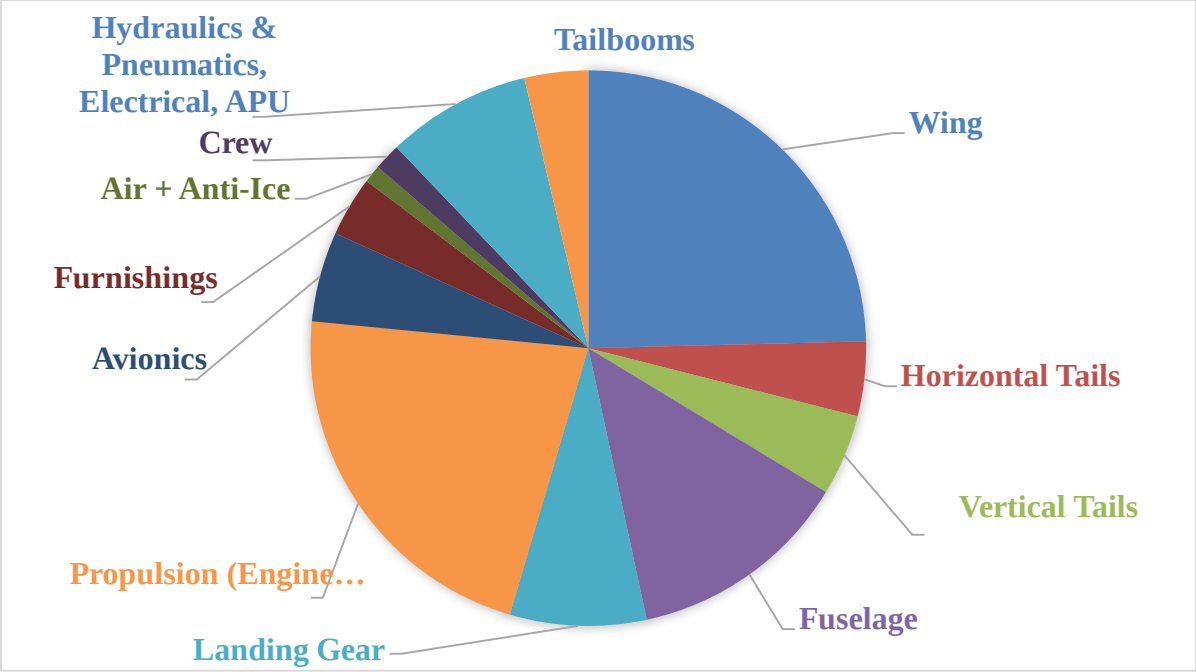

Figure 11-2: Detail weight percentage breakdown

11.1 CG Travel

After the weight breakdown, the C.G. location may now be determined by taking the weight moments for the individual elements on the group weight about the nose of the aircraft.

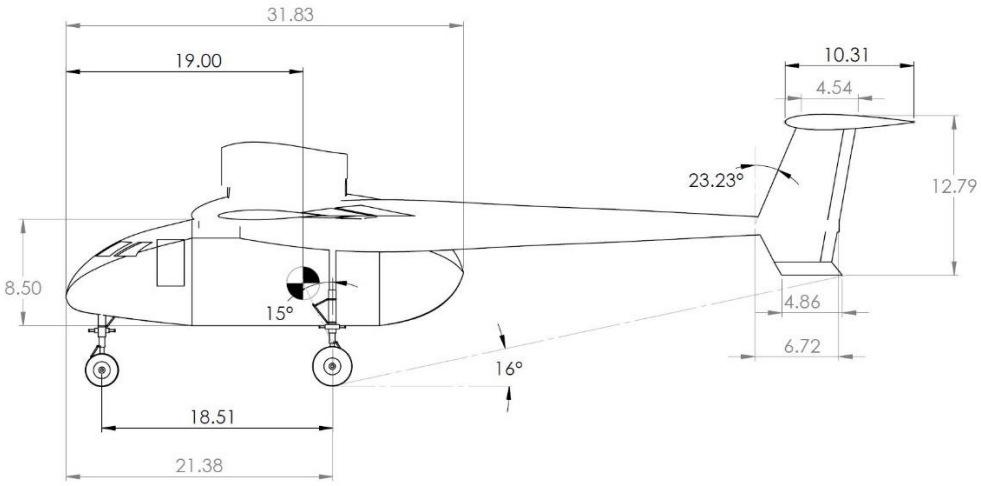

Figure 11.1-1: The CG shown when the aircraft is loaded with full fuel and full payload

The wing was placed in order to keep the CG stay in 25% to 35% of mean aerodynamic chord range

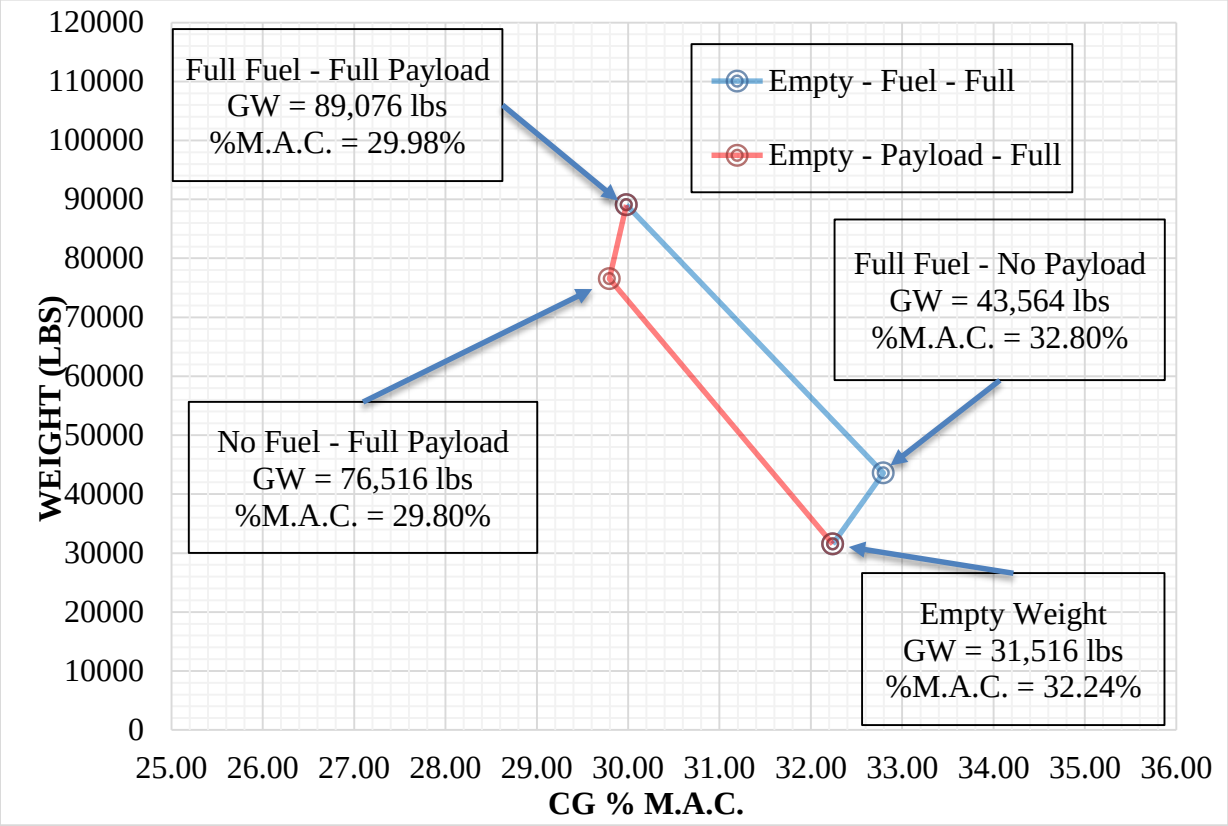

Figure 11.1-2: Balance Diagram

With the fuel (12,048 lbs) and retardant payload (45,000 lbs) weight added, the maximum takeoff weight are 89,076 lbs.

12. Structural Analysis

The LAT-1 structure was designed to withstand the most serious of the infinite number of possible combinations of external forces that may act on it in flight and in landing. The structural analysis began with the construction of the V-n diagram using the Federal Aviation Regulation (FAR) Part 25 guidelines. By using the guidelines from FAR Part 25, the design speeds for stall, cruising, diving, maneuvering, and maximum gust intensity were obtained and plotted them against the load factors. Overall, the combined V-n diagram was plotted as shown in Figure 12-1

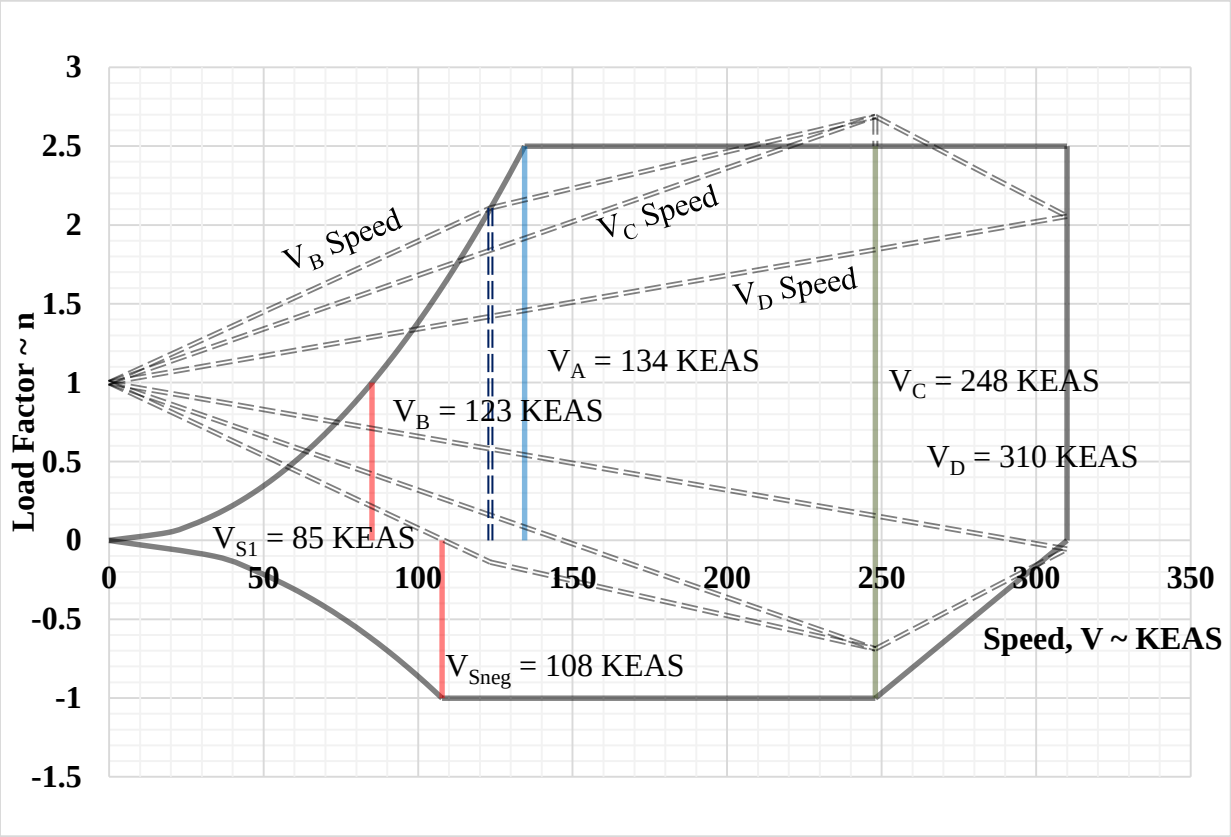

Figure 12-1: Combined V-n Diagram of LAT-1

The V-n diagram shows the design speeds and load factors for the aircraft in its clean configuration, without flaps or slats deployed. The maximum positive load factor predicted is 2.5 at maneuver and dive speeds while the maximum negative load factor is -1.

12.1 Wing Structure

First, the wing spanwise lift distribution was obtained from LinAir and input into Microsoft Excel to modify with the effect of engines and booms. By using method in Bruhn' book, the shear and bending moment diagram of the wing were constructed as shown in Figure 12.1-1 and Figure 12.1-2

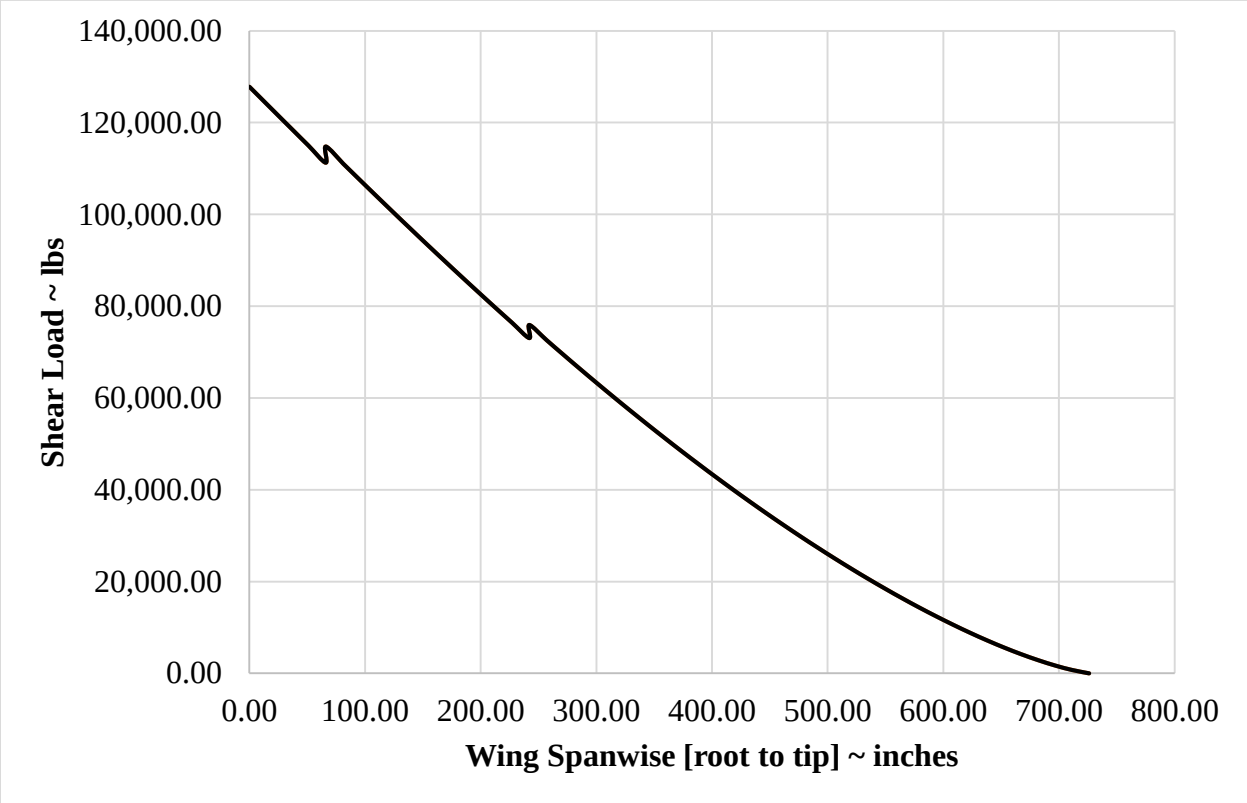

Figure 12.1-1: Spanwise Shear Loading of LAT-1 wing

This plot shows that at the wing root, the wing experiences 127,798 lbs of shear loading at the most extreme flight condition. Also, the engine and the boom on the wing help to reduce the shear load at the root chord. The plot below shows that the wing root experiences a moment 39,627,389 lbs-in at the most extreme flight condition.

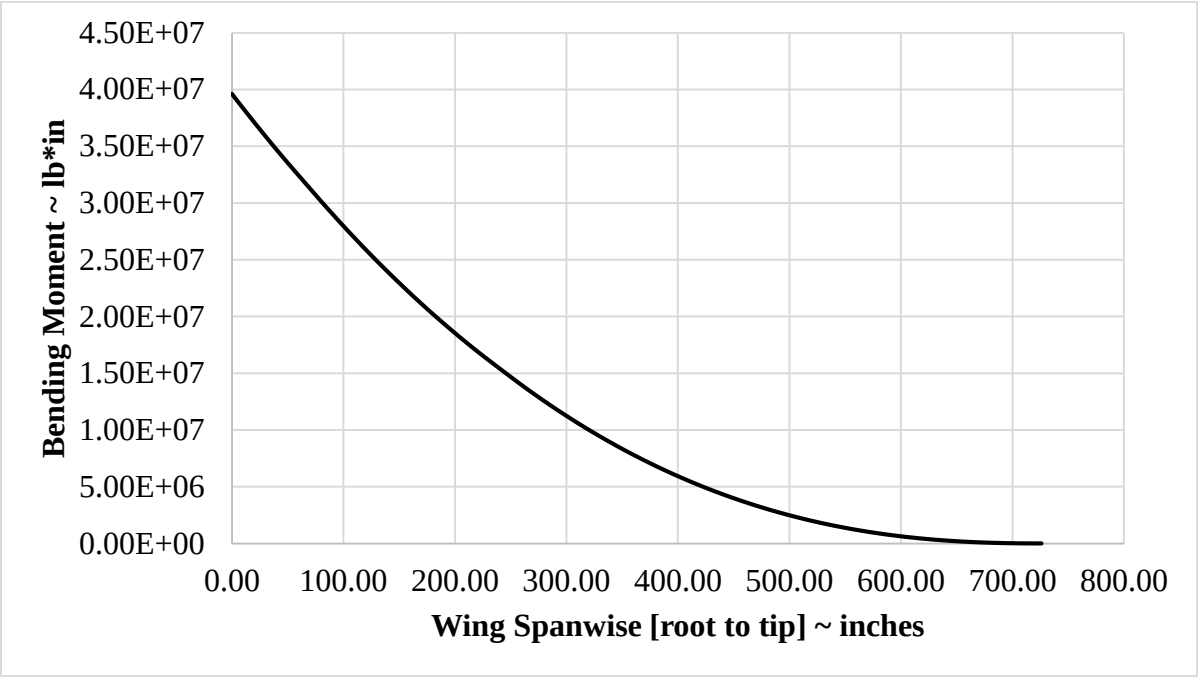

Figure 12.1-2: Spanwise bending moment in x direction of LAT-1 wing

Now, a safety factor 1.5 was applied to the shear and bending moment to size the wing spars. An iteration of spars and center pressure location were done to find the best combination location for the front spar and rear spar of the wing.

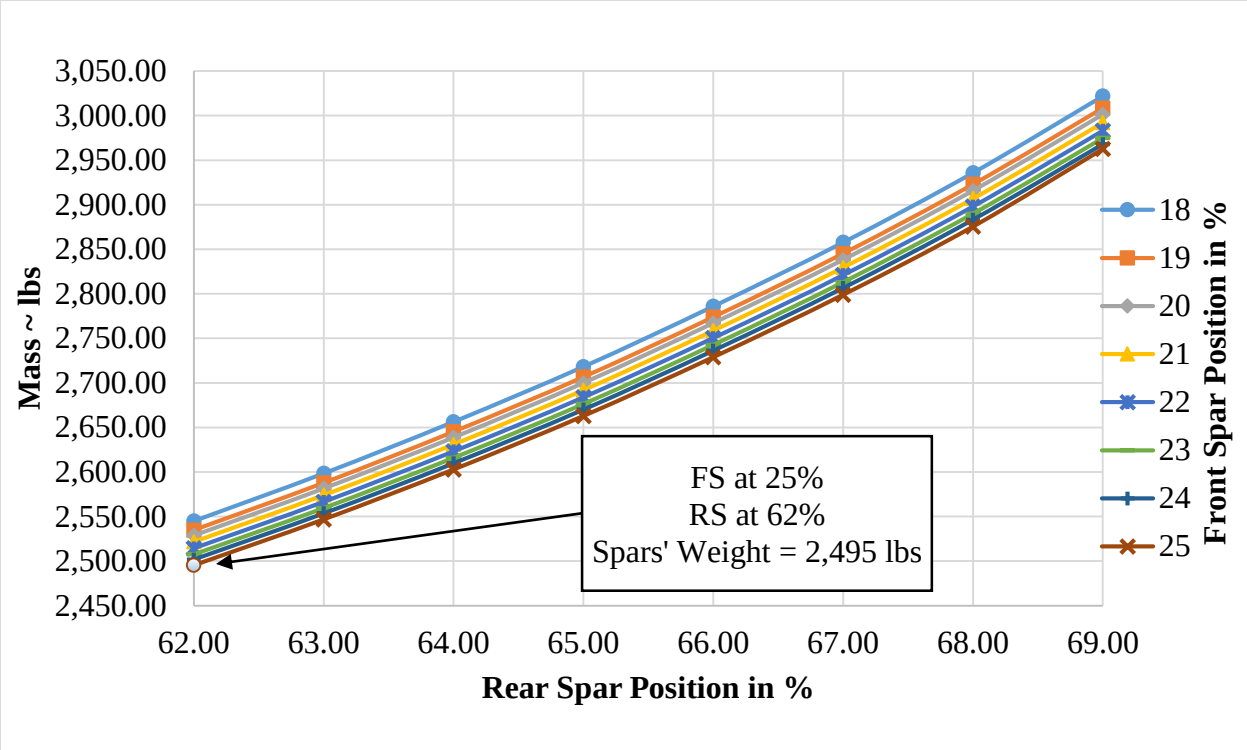

Figure 12.1-3: Spars Mass Calculation

The plot above shows that the (25% - 62%) combination of spars position was found suitable. The mas of this combination is 2,495 lbs which is least than any other combinations. Also, with this combination, 56% load will apply on the front spar and 44% on the rear spar.

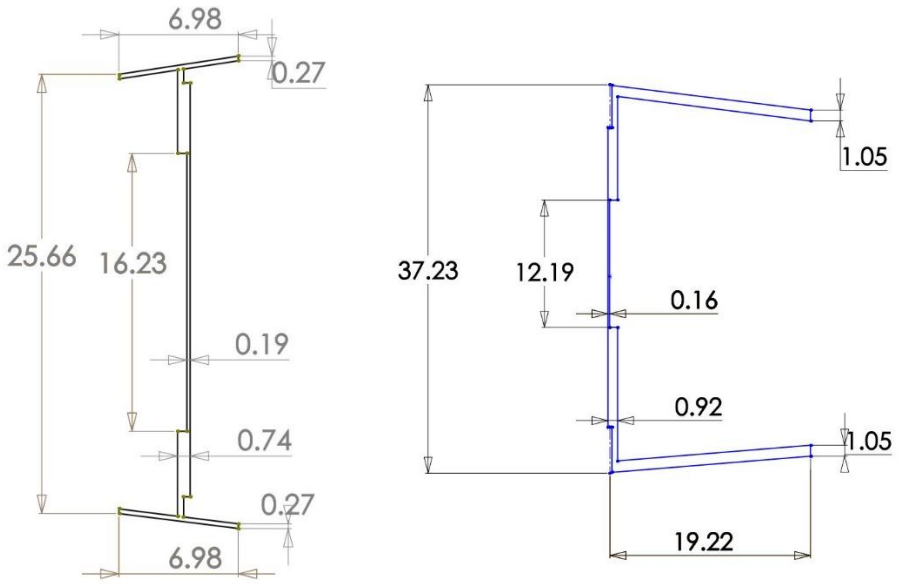

Figure 12.1-4: Front spar and rear spar dimension

Two L section for the flange, and web section for front spar. Two T section for the flange, and web section for the rear spar. Due to the RFP with fatigue attention, AA 2024 T3 was chosen to make the spars.

Table 12.1-1: Material Selection

Material AA 2024 - T3		
Ultimate tensile strength	70,000	psi
Shear strength	41,000	psi
Density	0.10	lb/in^3
Young's Modulus	10,600,000	psi
Poisson's Ratio	0.33	
Fatigue Strength (Endurance Limit)	20,000	psi

Also the lightening holes are made in the spars in order to reduce the weight of the spars. The crimp holes are made to the web element of the spar. These holes provided in between the two successive rib location.

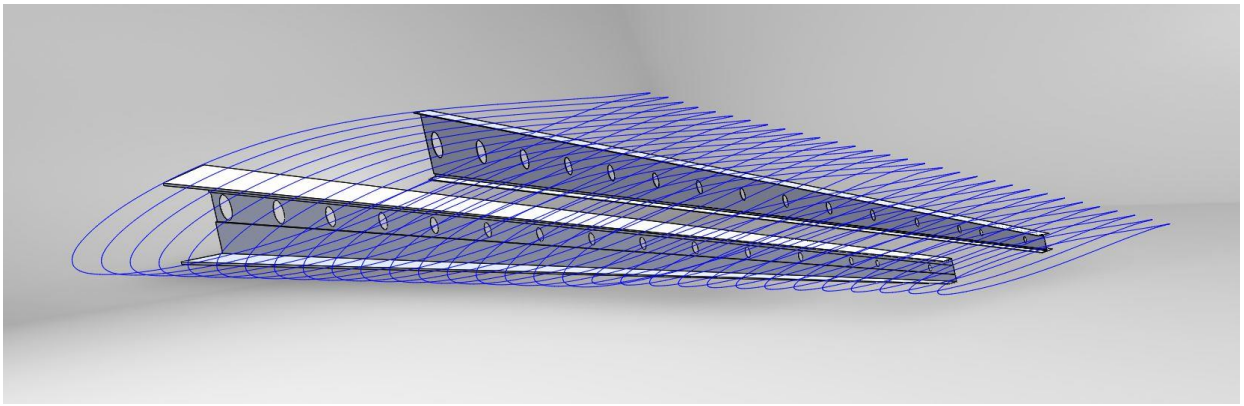

Figure 12.1-5 Spars with lightening holes

The ribs of the wing were placing 2 ft apart and sized to be 0.4 inches thick in order to withstand different scenario loads and minimize the weight of wing structural.

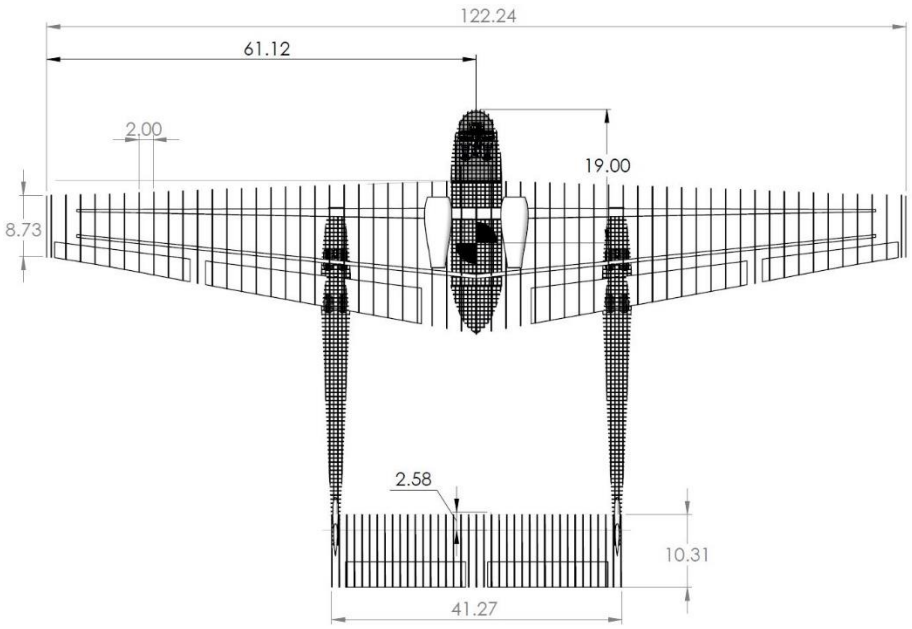

Figures 12.1-6: The internal wing structure includes front spar, rear spar and ribs

12.2 Fuselage Analysis

To analyze the shear and bending moment acting on the fuselage, the method mentioned in Bruhn's book was used. First, all the forces acting along the fuselage centerline were determined. Then, based on the location of the force with respect to the nose, the bending moment and shear forces were calculated. This calculation was done using excel; however, further precise calculation is needed to be done using Finite Element.

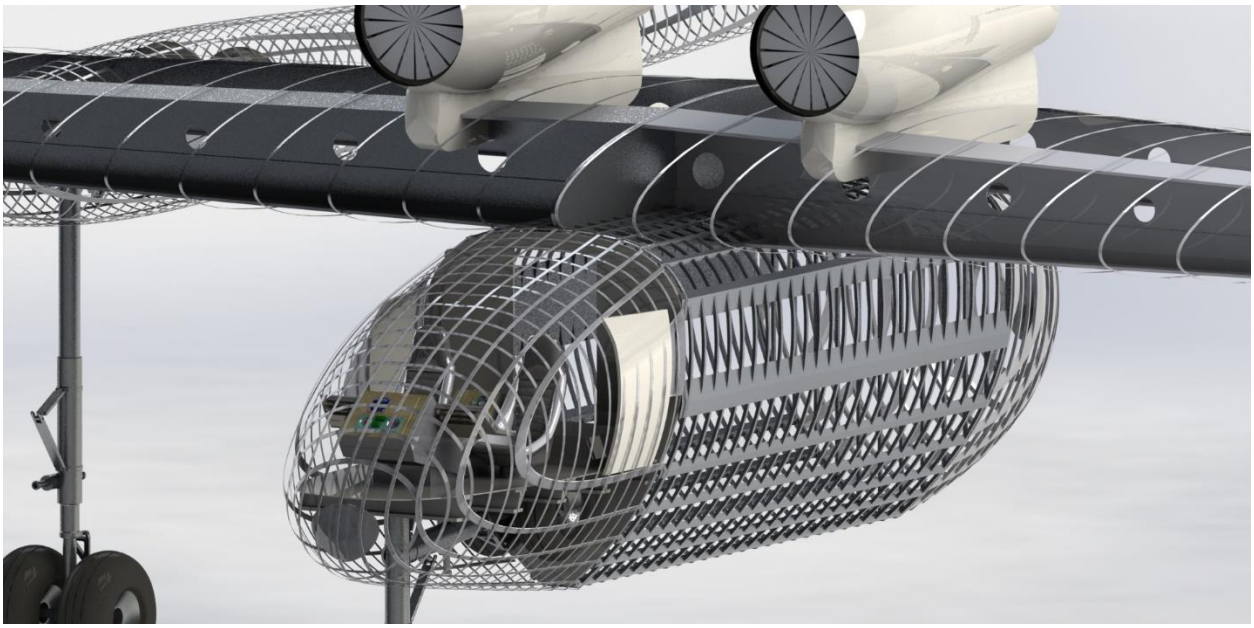

Figure 12.2-1: Structural layout of fuselage LAT-1

13. Landing Gear

The landing gear plays an important role in the world of aircraft's. The structural integrity of the landing gear allows the aircraft to land and takeoff smoothly. The landing gear supports the aircraft when it is not flying, when it is landing, when it is taking off, and when it is taxiing.

13.1 Landing Gear Placement

The best way to implement the landing gear in the aircraft is to know that the vertical CG should be no greater than 20% of the wing MAC above or below thrust line. Another thing to take into account is that the main landing gear location should not be greater than 20% ahead of and not less than 12% ahead of CG. Another thing to remember is that the weight of the nose gear needs to be between 8–15% of the total weight of the aircraft. In Figure 13.1-1 a vertical line drawn thru the aft main wheel and a diagonal line from the aft CG to the bottom of the aft wheel. An angle of 15° was obtained to be between the AFT CG line and the LG location.

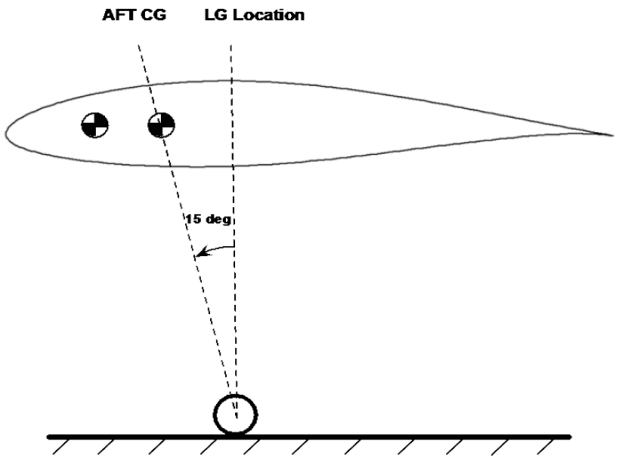

Figure 13.1-1: The angle between the AFT CG and the LG location is 15°

The main gears where placed 21.38 ft. from the nose to the main landing gear. The aircraft should also have a capable designed tip-back angle. The lowest point of the tail to the ground makes the tip-back angle. In Figure 13.1-2 we can see in red how we pick the lowest point of the tail and the ground to make the tip-back angle. The tip-back angle was determined to be 16°.

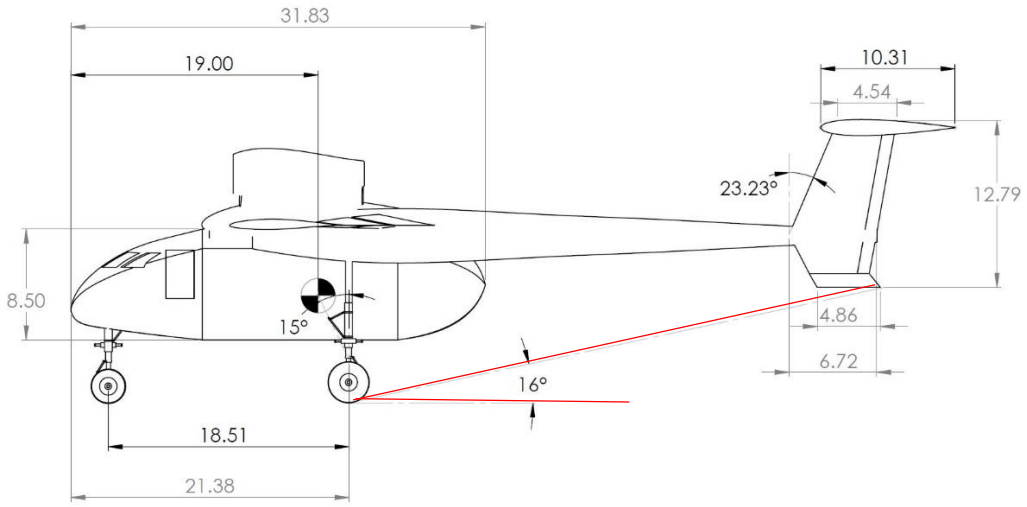

Figure 13.1-2: The tip-back angle was found to be 16°

The turnover angle requirements must also be meet in order to help the aircraft not turnover when doing high speed turns during taxiing. The turnover angle can be determined by using the method shown in Figure 13.1-3. It is desirable to keep the turnover angle as small as possible. By doing the calculations shown in Figure 13.1-3 we were able to determine a turnover angle of 36.8°. The requirements where meet since we did not surpass the maximum allowable overturn angle of 63°. The placement of the nose gear was 2.87 ft. from the nose of the aircraft to nose gear.

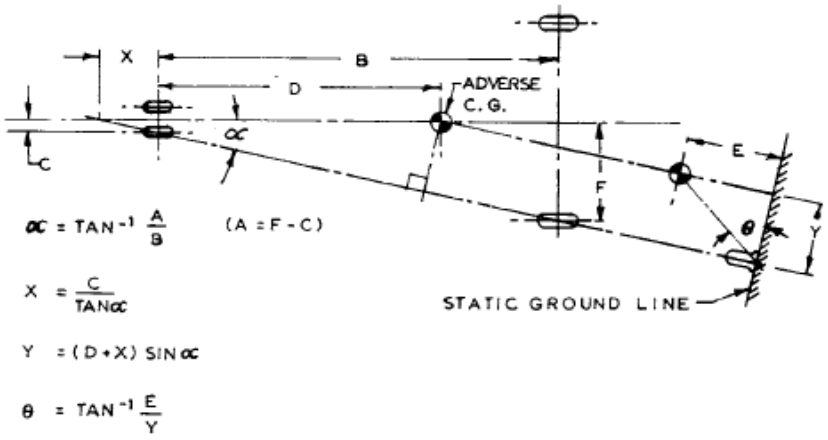

Figure 13.1-3: Over-turn calculations

In order to calculate the weight distribution between the nose gear and the main gear, calculations needed to be made. To find the maximum static main gear load we need to know the distance from the nose gear to the main gear and subtract it by the distance of the Aft CG to the main gear. Once that is done divide it by 2 times the distance of the nose gear to the main gear. Lastly multiply it by the weight and that will give you the maximum static main gear load. To obtain the maximum nose gear load we need to get the distance from the nose gear to the main gear and subtract it to the distance of the nose gear to the Fwd. CG. Once that is calculated divide it by the distance of the nose gear to the main gear and multiply all that by your weight to get your maximum static nose gear load. To determine the minimum static nose gear load we need to get the distance from the nose gear to the main gear and subtract it to the distance of the nose gear to the Aft CG. Once that is calculated divide it by the distance of the nose gear to the main gear and multiply all that by your weight to get your minimum static nose gear load.

13.2 Oleo Strut Sizing & Tire Selection

Once the landing gears where place we are able to pick appropriates tires that can handle the static loads. These tires were chosen to be 1.5 times the static load to withhold when the aircraft

is landing. In Figure 13.2-1 we can see the types of tires that were chosen with their diameter length. There are two tires for the nose gear with a diameter of 31.75 inches each and 4 tires for the main gear with a diameter of 38 inches each. These tires will help the aircraft maneuver smoothly.

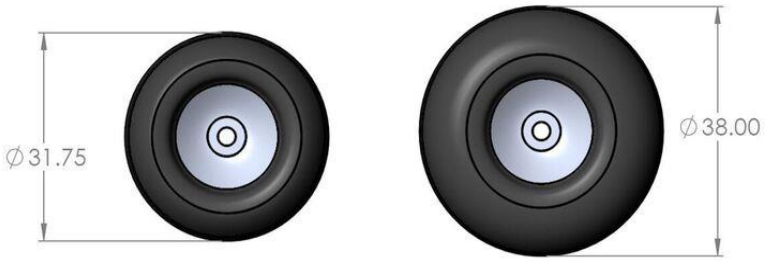

Figure 13.2-1: Chosen tires with its diameter

Oleo struts where the best fit for this aircraft. Oleo strut is a pneumatic air oil hydraulic shock absorber used on the landing gear of most small and large aircrafts. Oleo strut generally have a long operating live, which will save the company money on replacing the struts every year. The design of the oleo strut is designed to crush the impact of landing and damps out vertical oscillation. The design has a steel coil spring that will store impact energy and then releases it. As soon as the aircraft hits the ground an oleo strut absorbs this energy, reducing bounce. It is undesirable for the aircraft to bounce because it can lead to a loss of control. Finite Element was done on these struts to see if they can handle the stroke provided by the tires. In Figure 13.2-2 we can see a front view and a side view of the struts that were chosen to be in the nose gear and in the main gear.

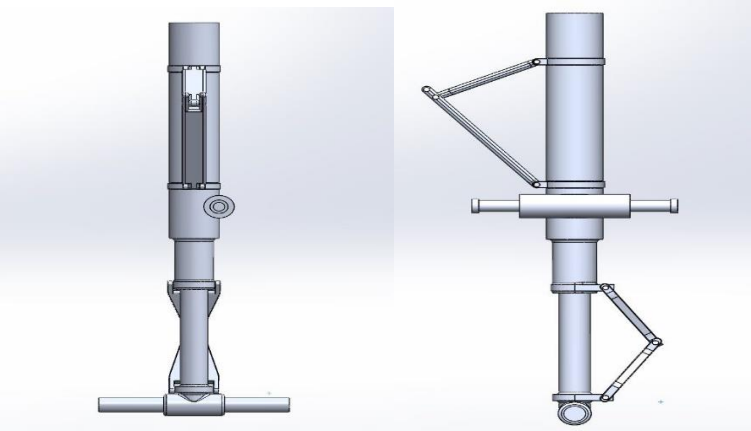

Figure 13.2-2: Front view and side view of oleo struts

13.3 Landing Gear Analysis

The purpose of using finite element on the landing gear is to determine the location of the maximum stresses. In order to analysis the landing gear tetrahedral elements where implemented. Constraints where applied on the top of the oleo strut to restrict the rotation and the translation between the attachment of the aircraft and the landing gear. In Figure 13.3-1 red indicates the location of the maximum stresses, for the worst case scenario using a load factor of 2.5.

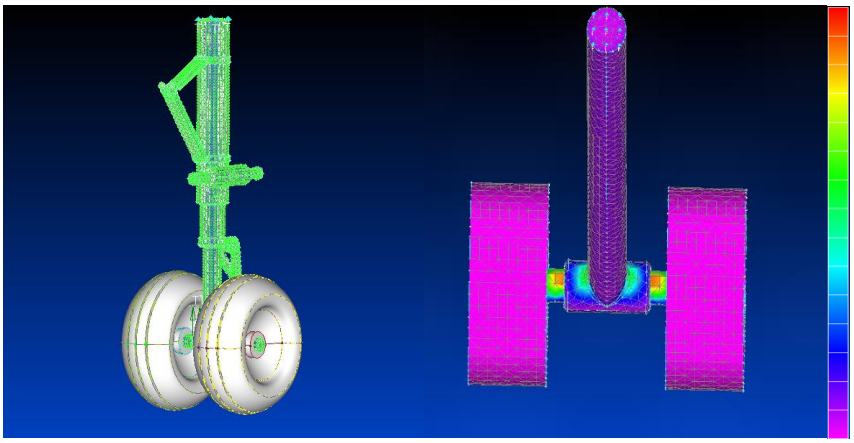

Figure 13.3-1: Finite Element Analysis of the landing gear

14. Fuselage Layout

The concept behind the fuselage layout is to reduce unnecassary empty space. There are two reasons, one to reduce structural weight, and two to have a simple, but efficient airplane. If we compare it with retrofitted aircraft like the the C-130 or the DC-10 which a small percentage of their fuselage volume is used to carry retardant; thereofore, making them less fuel efficient and costly to maintain.

14.1 Interior Fuselage Layout

The main cabin was design for two pilots with two exit doors at each side of the cockpit as shown in Figure 14.1-1. There is also a barrier between the tank and the cabin, with a door on the back of the cockpit for easy access during maintenace.

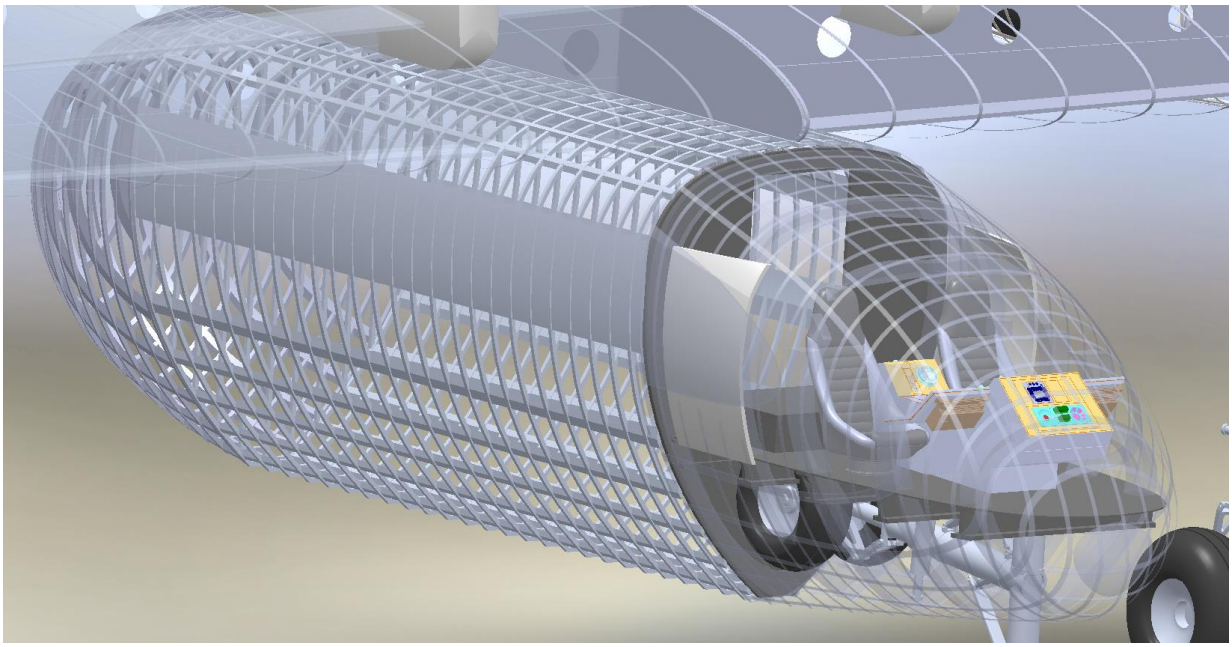

Figure 14.1-1: Interior cabin layout

14.2 Built-In Retardant Tank

The retardant tank has a volume of 5,000 gallons. To optimize fuselage volume, the airplane uses an integrated tank to carry retardant. As a plan to minimize unused empty space and reduce the weight of the aircraft for better performance. In Figure 14.2-1 shows the location and size of the retardant tank highlighted in red.

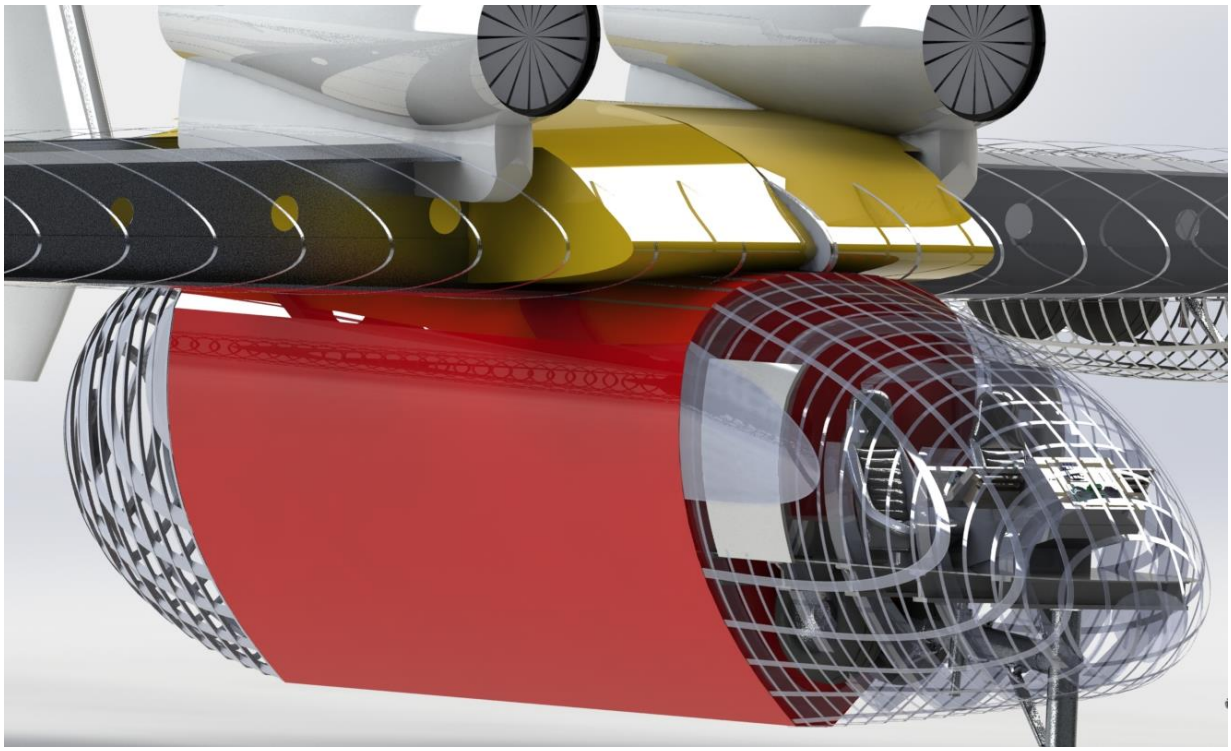

Figure 14.2-1: Retardant tank

14.3 Fuel

There will be two fuel tanks located inside the wing at the top of the fuselage highlighted in yellow in Figure 14.3-1 to meet the RFP requirement of an operational radius of 200 nm for one sortie carrying a full payload of 45,000 lb of retardant. The Breguet Range equation was used to calculate that the aircraft needed 382 gallons of standard JP-8 aircraft fuel. In order to meet the

RFP requirement for the ferry mission of 2,500 nm, 1,807 gallons of fuel is needed. The necessary volume for the aircraft fuel tank was calculated to be $256 ft^3$. The necessary fuel volume to meet the requirements mentioned above were calculated at 5,000 ft. above mean sea-level and at a temperature of 118 ˚F.

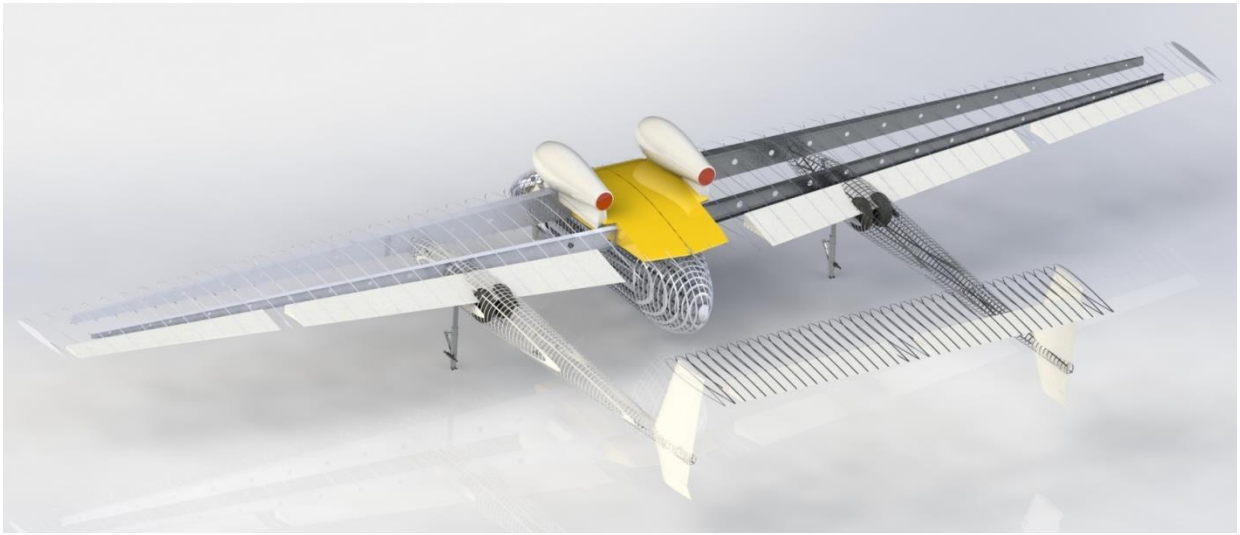

Figure 14.3-1: Fuel tanks located on the top of the fuselage

15. Maintenance

15.1 Airframe Maintenance

Firefighting aircraft typically operate in what can be considered a harsh environment, due to higher overall temperatures, airborne debris, strong updrafts and crosswinds, and consistently low altitude sorties over tall trees. Combining these operating conditions, the overall airframe structure is likely to be stressed more than typical commercial aircraft.

There are two main concerns in regards to airframe maintenance that are unique to this application. The first being debris impact, in which the aircraft flies lower than intended, and comes in contact with the upper canopy in and around the forest. The leading edge skin of the wing must be inspected on a regular basis for heavy impacts, tears, or rips in the aluminum skin. The second concern is corrosion. Due to the position of the door, it is a possibility the structure will be coated with fire retardant after a drop. This will require constant attention after every flight to ensure that the airframe is not oxidizing at a faster rate than what would be considered normal. Daily preflight inspections will help minimize this risk.

15.2 Engine Maintenance

Due to the harsh environment that this aircraft operates in, regular engine maintenance practices that take place on commercial aircraft are no longer stringent enough. It is not uncommon for tree branches up to 18 inches in length to become airborne due to strong gusts caused by rising heat and flames. The ingestion of heavy airborne ash from the fire is also likely to choke the engine of combustible oxygen, leading to an engine flame-out. Due to the increased rates of foreign object debris (FOD) ingestion, rotor blade damage throughout the engine core is significantly more likely

to occur on a regular basis, resulting in shortened maintenance cycles. These increased maintenance cycles lead to a higher operating cost over the lifespan of the aircraft, however are necessary to mitigate a possible catastrophic engine failure during a flight.

15.3 Retardant Tank Maintenance

Given that the payload tank is integrated into the fuselage in a wet manner, the airframe structure comes in direct contact with both water and fire retardant. While water itself can cause corrosion on an untreated 2024-T3 aluminum surface, fire retardant is far more corrosive if left in contact with an untreated surface. In 1986, the United States Department of Agriculture published a study titled, Guidelines for Preventing Fire Retardant Corrosion [4] that outlined the causes and prevention methods of corrosion due to contact between aluminum and magnesium and fire retardants. As was explained in this study, any 2024-T3 aluminum that would be submerged for periods of time in retardant needs either a metallic conversion coating, a barrier coating, or a combination of the two. The internal structure of the tank will be conversion coated with Alodine® 1201, after completion of assembly. Before each flight season, the internals of the tank must be sprayed with a paraffin based Tectyl type wax, to further mitigate corrosion, and to protect the surface conversion coating.

After each flight cycle/mission in which retardant is dropped, the payload tank will be flushed with water. If any retardant is allowed to solidify and gel, corrosion becomes an immediate risk. While flushing the tank after each flight day becomes wasteful, it is vital to maintaining a corrosion free airframe. In an attempt to prevent the wasting of water, the tank rinse water can be collected, and stored, to be mixed with more water and retardant concentrate for subsequent flights. Once weekly, the payload tank shall be inspected to look for any signs of gelled retardant, and any

obvious corrosion. In the event of a break in the conversion coating, or untreated aluminum being discovered, a technician must enter the payload tank, and repair the break in the Alodine® surface treatment, through the use of an Alodine® repair pen.

In addition to the repair and maintenance of the internal structure of the tank, special care must be taken to inspect and service the fluid drop doors. These doors precisely meter the flow pattern and mass flow of the fluid as it is dropped from the aircraft, therefore proper maintenance is vital to ensuring a successful drop. All operating linkages shall be inspected and lubricated as necessary before each flight, immediately before the tank is refilled.

16. Subsystem

16.1 Water/Retardant Filling Methods

The payload refilling process is required to occur within a period of no more than 10 minutes, with engines idling on the tarmac. To achieve this, a high flow-rate pump had to be selected and configured to interface properly with the payload tank. The selected pump was a Waterous CXK centrifugal pump, with an internal gearbox for ensuring proper impeller RPM. The pump is designed to operate within a viscosity range of 0.28 to 65 mPa·S (Approximately ranging from water to SAE 10W motor oil) while producing a 1,500 GPM flow rate at peak output, leading to an approximate fill time of 3.5 minutes. Operating the pump at peak conditions is not recommended by the manufacturer however. Operating at a 70% condition, the pump will successfully fill the tank in under 5 minutes, thus allowing 5 minutes for the technician to engage the pump, and connect fill hose from the pump cart to the aircraft tank, as well as inspecting the fluid drop doors.

Hose couplings between the pump apparatus and the aircraft must be large enough to not limit the flow rate of the pump, and must also seal in a manner that prevents the leaking of fluid when removed due to the semi-corrosive properties of the fire retardant. Our solution to this problem is a large diameter Dry-Brake® connection, a fitting type well established in the petrochemical and auto racing industry. The selected 119mm diameter fittings are shown below in Figure 16.1-1.

Figure 16.1-1: Rakord TODO-Matic® 119mm Dry-Brake® Fitting

A secondary vent/vacuum system was also implemented on the top side of the tank to not only allow the tank to passively regulate internal pressure changes inside the tank due to changing ambient conditions on the tarmac, but to also aid in the flow rate of a large fluid tank. A vacuum pump will simultaneously be operated in conjunction with the fluid pump, to apply a relative vacuum to the entire payload tank. This ensures that any air in the tank being displaced by the fluid is being evacuated, and that no pressure builds up inside the tank during the filling operation. Dry-Brake® couplings will be implemented for this operation as well, in the event that the tank is overfilled and fluid must be expelled out of the tank vents.

16.2 Auxiliary Power Unit

Due to the use of turbofan engines, and the likelihood of operating the aircraft out of an unimproved runway/ operating base, an auxiliary power unit (APU) was deemed a necessary ancillary device. At an unimproved runway, there is little chance an air cart will be available for use of starting the engine, which therefore leaves an APU as the only starting method [3]. Given the *size zero* mindset that is being applied to the entire aircraft, the decision was made to place the APU in the aft fairing that is used to blend the payload tank into an aerodynamic shape. This not

only utilizes the empty space created by the fairing, but also allows for a simple and effective exhaust vent at the tail of the fairing. Given the size constraints of the aft fairing, our selection was limited to auxiliary power units in use on small regional passenger aircraft. The APU that was chosen for this application was the UTC Aerospace APS-500R. It weighs approximately 120 lbs. dry, and includes an FAA TSO C77A certified full authority digital engine controller (FADEC) unit, and is more than capable of starting our selected GE CF34 series engine. The dimensions of this APU are shown below in Figure 16.2-2.

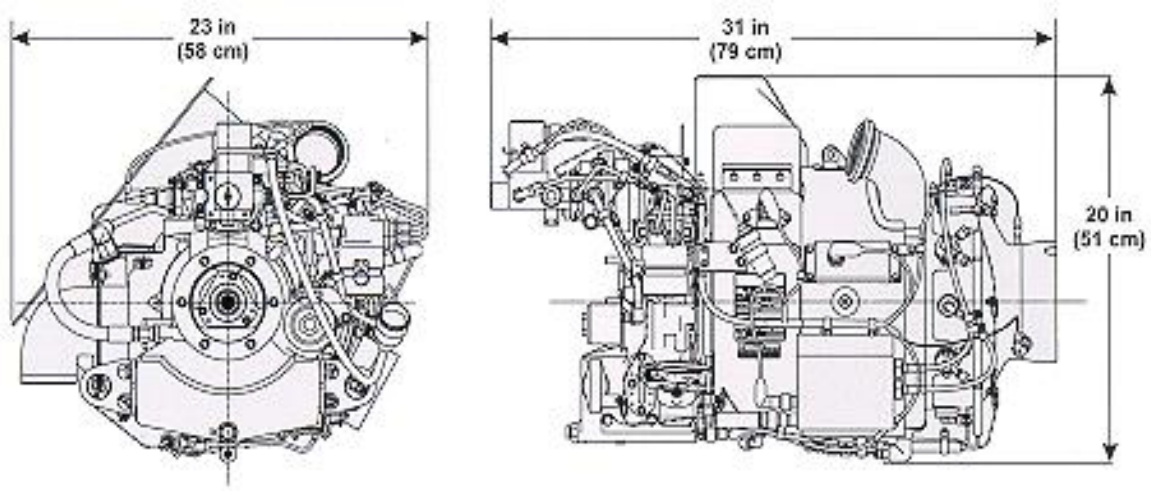

Figure 16.2-2: UTC APS-500R APU Dimensions

16.3 Supplemental Oxygen

Since the aircraft contains only two crew and no passengers, pressurization is unnecessary and would only lead to increased fuselage weight and fatigue. However, flight at altitudes greater than 12,500 feet MSL is still expected so some form of supplemental oxygen is required. This supplemental oxygen will be generated by a molecular sieve oxygen generator (MSOG). An MSOG eliminates the need for heavy, bulky, pressurized tanks that only store a limited amount of oxygen since it concentrates the oxygen from the ambient air.

This oxygen is delivered to the pilots using diluter-demand masks which only supply oxygen during inhalation, making them very efficient. They also dilute the oxygen with the ambient cabin air to ensure the proper oxygen percentage at any altitude up to 40,000 feet MSL.

16.4 Situational Awareness

Our design features several cameras located throughout the airframe to improve situational awareness. One of these cameras will be a forward looking infrared (FLIR) camera. Infrared cameras would allow the pilots to see obstacles and terrain through dense smoke that would otherwise obscure their vision. Three more visible light cameras will be located in the tail and each wingtip. These cameras are for providing spatial awareness and to help the pilots gauge their clearance from obstacles when flying at low altitude and during ground operations at small airports.

17. Cost Analysis

One of the most important requirements mentioned in the RFP is to minimize cost. Since there are fire fighters currently operating, the cost of the new design should be lower than the existing ones. According to the RFP, the aircraft should enter into service in 2022; therefore, the cost analysis was done for 2022 U.S. dollars. To take into account the inflation rate, equation 1 was used.

$$X_{Inflated} = X_{current} * 1.031^{(2022\text{-Current Year})} \qquad \textbf{Equation 17-1}$$

In order to do the cost analysis two methods were used, Nicolai & Carichner [2] and Raymer [5].

17.1 Research, Test, Development and Evaluation Cost

Using the Nicolai & Carichner's method the total Research, Test, Development and Evaluation (RTD&E) cost was calculated to be $4.5 billion in 2022 U.S. dollars, and using Raymer's method, the RTD&E cost was $3.6 billion. The RTD&E cost breakdown, shown in Figure 17.1-1 is based on the MTOW and the maximum speed of the aircraft for a total of 100 aircraft produced for testing and analysis.

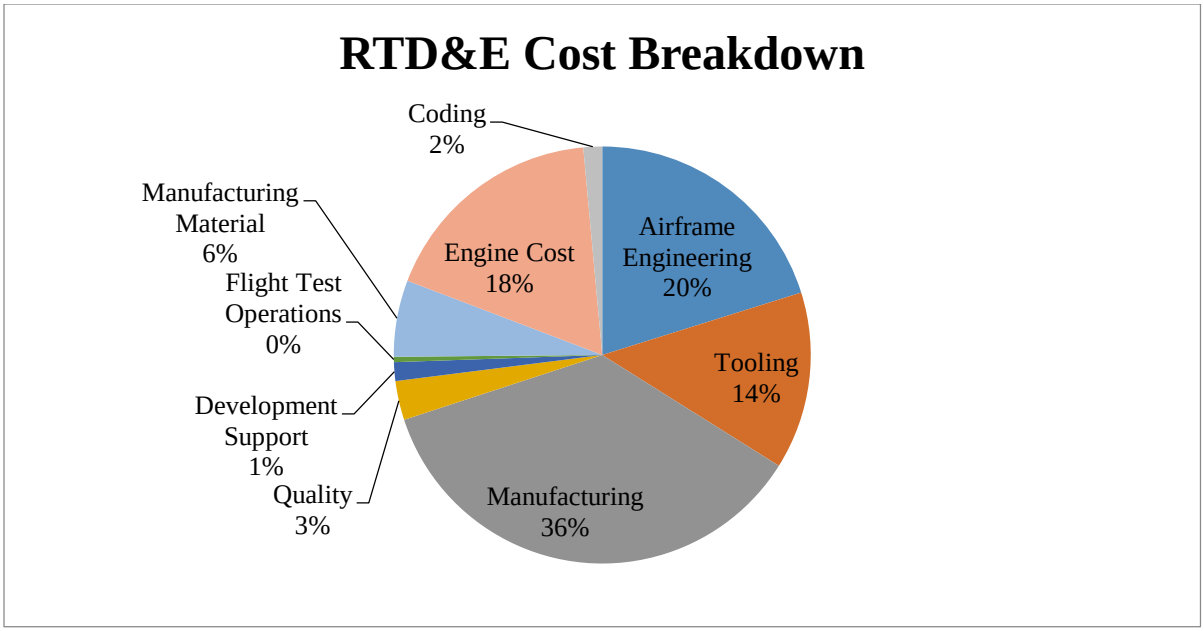

Figure 17.1-1: RTD&E cost breakdown

17.2 Flyaway Cost

Flyaway cost or production cost includes the airframe, engine, and avionics. It is calculated by dividing the total production cost by the number of aircraft produced. The results for Nicolai & Carichner and Raymer's method are $45 million and $36 million (per unit), respectively. The breakeven point for Nicolai & Carichner's method is 79 aircraft, shown in Figure 17.2-1, and for Raymer's method it is 76 aircraft, shown in Figure 17.2-2. The breakeven point was calculated assuming a 12% profit margin.

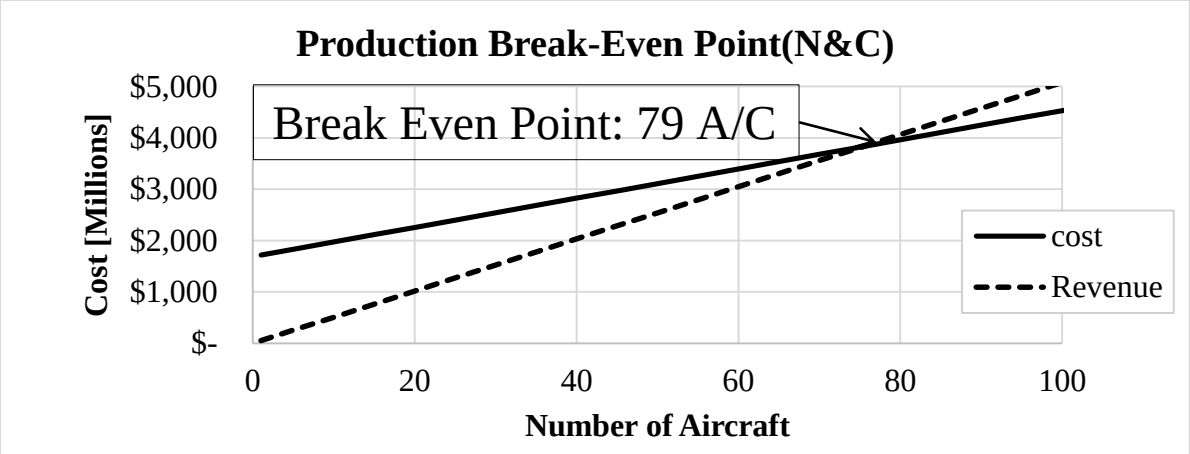

Figure 17.2-1: Production breakeven point using Nicolai & Carichner's method

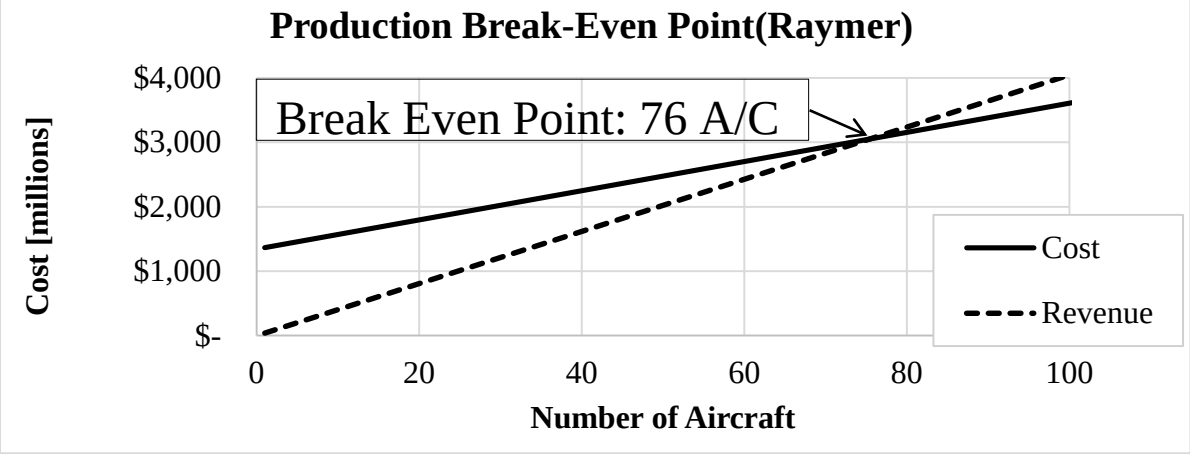

Figure 17.2-2: Production breakeven point using Raymer's method

17.3 Direct Operating Cost

The Direct Operating Cost (DOC) was also calculated using Nicolai & Carichner's method. The calculation was based on the MTOW, the net thrust at SSL for all engines, the number of crew, and the distance the aircraft will travel. However, besides all these cost drivers mentioned, fuel cost and retardant cost make the majority of the expenses. The operational cost per mission for this design was calculated to be $22,970. This result was compared to the DC-10's with the total of $23,018 hourly flat rate, which is the twin turbofan engine aircraft currently operating with

the lowest rate. With this result our design is more economical. Figure 17.2-1 shows the breakdown of the operational cost.

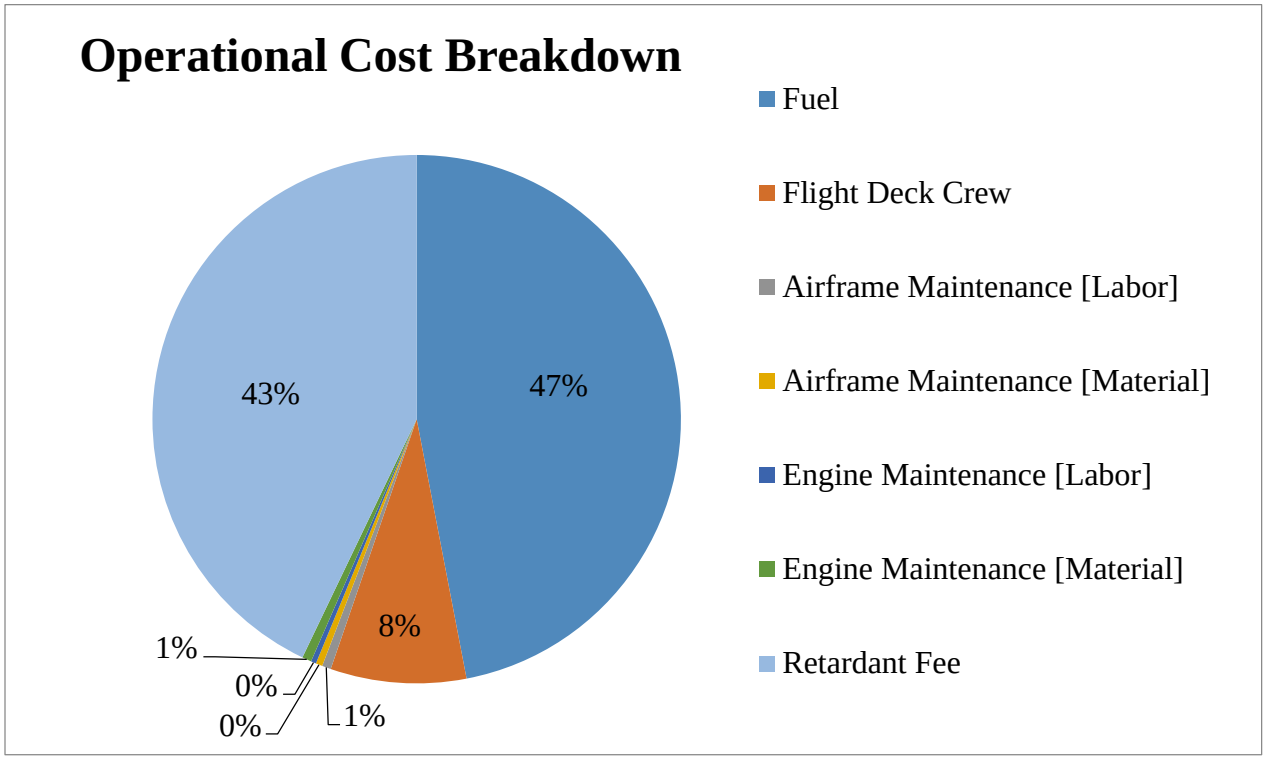

Figure 17.3-1: Operational cost breakdown

18. Manufacturing Concepts

The manufacturing process for our aircraft will follow that for other small volume aircraft production lines. Our company plans to purchase all subsystem components from only American companies, and to create subcontractor relationships with those American companies. The focus placed on purchasing from American companies carries over to the purchasing of raw materials, in an effort to control the quality of material being used in the manufacturing of large structural components such as the wing spars.

Due to the low production volume predicted for such a specialized aircraft, developing a production-assembly line is most likely not necessary, and just not justify the significant investment. Instead, our team plans to attract a small group of well trained technicians that are capable of manufacturing multiple types of components. This will not only keep costs down, but with a smaller group of more talented technicians, we can ensure a higher quality product for the USFS.

In an effort to control the high quality that we expect for our aircraft, thorough inspections will be performed at every stage in the manufacturing process. It is significantly cheaper to catch a manufacturing flaw in the early manufacturing stages. Each aircraft will also be flight tested for no less than 20 hours to ensure a proper operation of the aircraft when it is finally delivered.

19. Acoustics & Environment

Ember Aviation is not only a proud firefighting company; it takes into consideration the emissions the aircraft releases to the environment as well as the retardant it leaves behind when it the aircraft is fighting fires. With this in mind, Ember Aviation's LAT-1 is equipped with 2 turbofan General Aviation engines: the CF34-8E.

The engines selected have met or surpassed the International Civil Aviation Organization (ICAO) Chap. 4 requirements. These requirements are important because they limit, or reduce, the number of people that are affected by the significant aircraft noise. It is important to keep this in mind because even though the LAT-1 will be fighting wildfires, Ember Aviation wishes not to discomfort any humans that may be near the wildfire. In addition, the engine also meets or surpasses the ICAO Committee on Aviation Environmental Protection (CAEP) requirements. This requirement states that the emissions released by the aircraft should limit the contamination it releases into the atmosphere. It should maintain good local air quality with the emissions released form the engine. When it comes to dropping the retardant, it is important to clean-up the debris that will be left behind. Since wildfires can occur anywhere if for people get contaminated with the retardant, they must wash thoroughly with gentle soap and rinse with water because retardant contains ammonia and may cause a sting or drying of the skin. It is also recommended to use good quality hand cream on your body to minimize the drying and chapping on the skin. Wildfires are most commonly experienced in forest areas, and the retardant that is dropped will contaminate the vegetation around the fire site. Once the fire is defeated, it is extremely important to rinse off the vegetation with fresh water to prevent it from dying. Leaf burn from vegetation may occur since the retardant is more dense with fertilizer than compared to that of local garden stores; however, they will recover and grow back usually within one or two months.

20. Program Lifecycle

The Program Lifecycle is broken down into 7 milestones that are illustrated in Figure 20-1

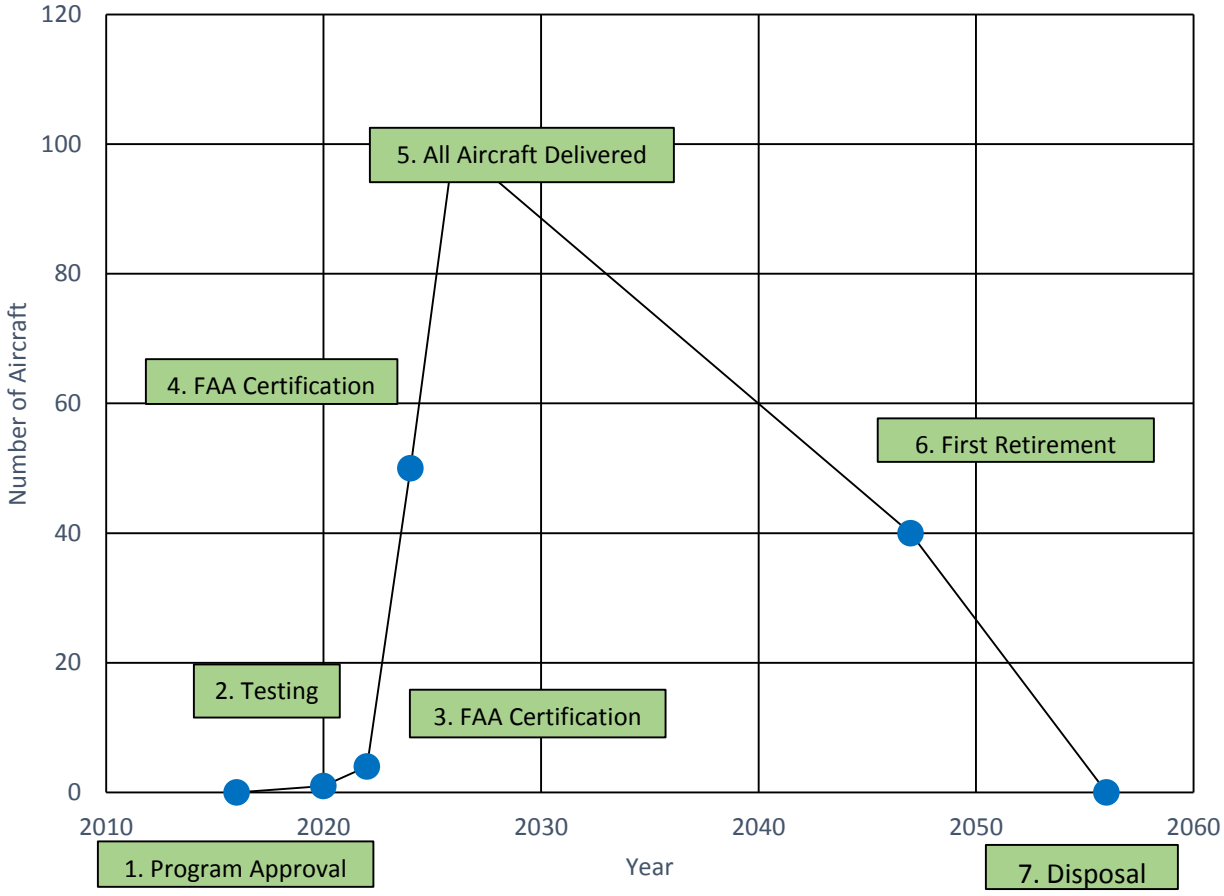

Figure 20-1: LAT-1 Program Lifecycle

To begin the Program Lifecycle, the program approval is scheduled for August 2016. After the approval, the contract will be awarded and commencement of manufacturing will proceed. A full scale of the aircraft will be produced in 2020 for testing of the unique fuselage configuration along with testing of the hydraulic systems that will be actuating the door to perform the retardant drops and other features that the aircraft will include. In the year of 2021, the FAA certification tests will be scheduled. After certification from the FAA, the aircraft assembly line can run in full

effect. The first lot of 4 aircraft will be delivered in the year of 2022 as requested by the customer. Ember Aviation will be delivering 2 aircraft per month once the first lot has been delivered. The whole fleet of aircraft is projected to be completed and delivered by the year of 2026. It is estimated that the aircraft will have a lifespan of 25-30 years. Disposal of the program will initiate in 2047 and they will be out of service by the year of 2056. All aircraft will be sent to AFRA (Aircraft Fleet Recycling Association) where they will be either retired, recycled, or scrapped for parts.

21. Compliance Matrix

Req.	Requirement Description	Met (Y/N)	Comments
1	Ferry Range of 2,500 nm	Yes	Addressed in Payload Range Curve
2	Crew 2 pilots	Yes	Addressed
4	Stall Speed of 90 knots	Yes	Addressed in V-n diagram 86 knots
5	Dash Speed greater than 300 knots	Yes	Addressed in Operation Envelope
6	Payload of 5,000 gallons fire retardant or water	Yes	Addressed, adequate retardant tank
7	Drop Altitude less than 300 ft. AGL	Yes	Addressed in Operational Envelope
8	Retardant Reload of 10 minutes	Yes	Addressed, adequate pump selected
9	Balanced Field Length of 5000 ft. for FAR 25	Yes	Addressed in Balance Field Length 4,980 ft.
10	Operational Radius of 200 nm	Yes	Addressed in Payload Range Curve
11	Drop Speed Below 150 knots	Yes	Addressed, low stall speed
12	Turboprop or Turbojet Engine	Yes	Turbofan CFE-8E

22. Conclusion

The LAT-1, designed by Ember Aviation in response to AIAA's RFP for a 2022 Large Air Tanker for Wildfire Attack, meets all the requirements from the RFP. With the prediction of increasing wildfires, the LAT-1 meets the need of having a purposely built firefighting aircraft compared to a retrofitted aircraft. The LAT-1 is built from the ground up for firefighting purposes. It includes features such as a retardant tank shaped fuselage to prevent having unnecessary empty space in the fuselage, unpressurized structure to make the aircraft lighter and less vulnerable to fatigue, wide range cameras to assist the pilots with their view, and Forward Looking Infrared (FLIR) cameras to assist the pilots as they fly in smoke heavy atmosphere. Being built from the ground up specifically as an air tanker, the LAT-1 allows for an efficient and mission driven design.

References

[1] Schrock, Erich. "Aircraft Design Approaches." Senior Design Lecture. Cal Poly Pomona, Pomona. Lecture.

[2] L. M. Nicolai and G. E. Carichner, Fundamentals of Aircraft and Airship Design, Vol. 1, American Institute of Aeronautics and Astronautics, Inc., 2010.

[3] R. D. Schaufele, Elements of Aircraft Preliminary Design, Santa Ana, California: Aries Publications, 2007.

[4] Gehring, George A., Jr., and Charles W. George. "Guidelines for Preventing Fire Retardant Corrosion." *United States Department of Agriculture* INT.210 (1986): n. pag. Web.

[5] D.P. Raymer, Aircraft Design: A Conceptual Approach, Washington, D.C.: AIAA, 1992.

[6] M. Sadraey, Aircraft Design: A Systems Engineering Approach, Wiley Publications, September 2012.

[7] M.Drela, "Development of the D8 Transport Configuration," in 29th AIAA Applied Aerodynamics Conference, Honolulu, HI, 2011.

[8] Roskam, J. "Methods for estimating drag polars of subsonic airplanes". Roskam aviation and engineering corporation, 519 Boulder, Lawrence, Kansas 66044, (1973).

[9] Roskam, J. "Methods for estimating stability and control derivatives of conventional subsonic airplane". Roskam aviation and engineering corporation, 519 Boulder, Lawrence, Kansas 66044, (1973).

[10] Wood, K.D., "Aerospace vehicle design Vol.I." Johnson Publishing Co. Boulder Colorado, U.S.A, (1966)

[11] Abbot, I.H and Von Doenhoff, A.E., "Theory of wing sections", Dover, (1959).

[12] Roskam, J. “Airplane design Volumes I to VIII”. Roskam aviation and engineering corporation, 519 Boulder, Lawrence, Kansas 66044, (1973).

[13] Heffley R.K and Jewell, W.F, “Aircraft handling qualities data”, NASA CR 2144(1972). This report can be downloaded from “NASA Technical Report Server (NTRS)”

[14] Conway, H. G., Landing Gear Design, Chapman & Hall, London, 1958.

[15] Currey, N. S., Aircraft Landing Gear Design: Principles and Practices, AIAA Education Series, Washington, 1988.

[16] Niu, M. C. Y., Airframe Structural Design, Conmilit Press, Hong Kong, 1988, pp. 430-470

[17] Anon., FAR Part 25 Airworthiness Standards: Transport Category Airplanes, Federal Aviation Administration, Washington, DC, October 1994.

[18] Beer, F. P. and Johnston, Jr., E. R., Mechanics of Materials, 2nd ed., McGraw-Hill, New York, 1992, pp. 610-616

[19] Megson, T. H. G., Aircraft Structures, 2nd. ed., Halsted press, New York, 1990, pp. 225-293.